Multi-proxy record of Holocene paleoenvironmental conditions from Yellowstone Lake, Wyoming, USA

Authors:

Sabrina R. Brown*[1,2], Rosine Cartier[3], Christopher M. Schiller[4**], Petra Zahajská[3,5], Sherilyn C. Fritz[1], Lisa A. Morgan[6], Cathy Whitlock[4], Daniel J. Conley[3], Jack H. Lacey[7], Melanie J. Leng[7,8], W.C. Pat Shanks III[6]

*Corresponding author: email: sabrown@defiance.edu, 701 N Clinton St, Defiance, OH 43512

1 Department of Earth and Atmospheric Sciences, University of Nebraska-Lincoln, Lincoln, NE 68588, USA

2 Division of Natural Science, Applied Science, and Mathematics, Defiance College, Defiance, OH 43512, USA

3 Department of Geology, Lund University, Sölvegatan 12, 22362, Lund, Sweden

4 Department of Earth Sciences, Montana State University, Bozeman, MT 59717, USA

5 Institute of Geology and Paleontology, Charles University, Albertov 6, Prague, 12843, Czechia

6 U.S. Geological Survey, Denver Federal Center, MS 973, Denver, CO 80225-0046, USA

7 National Environmental Isotope Facility, British Geological Survey, Nottingham, NG12 5GG, UK

8 Centre for Environmental Geochemistry, School of Biosciences, University of Nottingham, Nottingham, LE12 5RD UK

** Now at Department of Biology, University of Washington, Seattle, WA 98195, USA

Abstract

A composite 11.82 m-long (9876–-67 cal yr BP) sediment record from Yellowstone Lake, Wyoming was analyzed using a robust set of biological and geochemical proxies to investigate the paleoenvironmental evolution of the lake and its catchment in response to long-term climate forcing. Oxygen isotopes from diatom frustules were analyzed to reconstruct Holocene climate changes, and pollen, charcoal, diatom assemblages, and biogenic silica provided information on terrestrial and limnological responses. The long-term trends recorded in the terrestrial and limnic ecosystems over the last 9800 years reflect the influence of changes in the amplification of the seasonal cycle of insolation on regional climate. The early Holocene (9880–6700 cal yr BP) summer insolation maximum and strengthening of the northeastern Pacific subtropical high-pressure system created warm dry conditions and decreasing summer insolation in the middle (6700–3000 cal yr BP) and late (3000–-67 cal yr BP) Holocene resulted in progressively cooler, wetter conditions. Submillenial climate variation is also apparent, with a wetter/cooler interval between 7000 and 6800 cal yr BP and warmer and/or drier conditions from 4500 to 3000 cal yr BP and at ca. 1100 cal yr BP. These data show that the Yellowstone Lake basin had a climate history typical of a summer-dry region, which helps to better define the spatial variability of Holocene climate in the Greater Yellowstone Ecosystem.

Keywords

pollen, charcoal, diatoms, biogenic silica, oxygen isotopes, paleoclimate

1. Introduction

As the largest intact temperate ecosystem in the world, the Greater Yellowstone Ecosystem (GYE) is composed of diverse terrestrial and aquatic environments (Keiter and Boyce, 1994). These environments have been sensitive to climate changes occurring on different temporal and spatial scales since the last ice age, as demonstrated by paleoecological studies of both small and large lakes in the region (Fritz and Anderson, 2013; Huerta et al., 2009; Iglesias et al., 2018; Millspaugh et al., 2000; Theriot et al., 2006; Whitlock, 1993; Whitlock et al., 2012).

Yellowstone Lake (44°30′N, 110°20′W; 2350 m elevation; Fig. 1), in the center of the GYE, is the largest alpine lake in North America, with a surface area of 344 km^2 and maximum depth of ~119 m (Cash, 2015; Morgan et al., 2003). The watershed of Yellowstone Lake was covered by a large late-Pleistocene glacier complex until ca. 14 ka (Licciardi and Pierce, 2018) and has since been influenced by hydrothermal activity in the northern and West Thumb portions of the lake, as evidenced by heat flow patterns (Bouligand et al., 2020; Morgan et al., 1977; Smith et al., 2009; Morgan et al., 2007a), subaqueous vent fields and large explosion craters and domes (Balistrieri et al., 2007; Johnson et al., 2003; Morgan et al., 2003, 2007b, 2009).

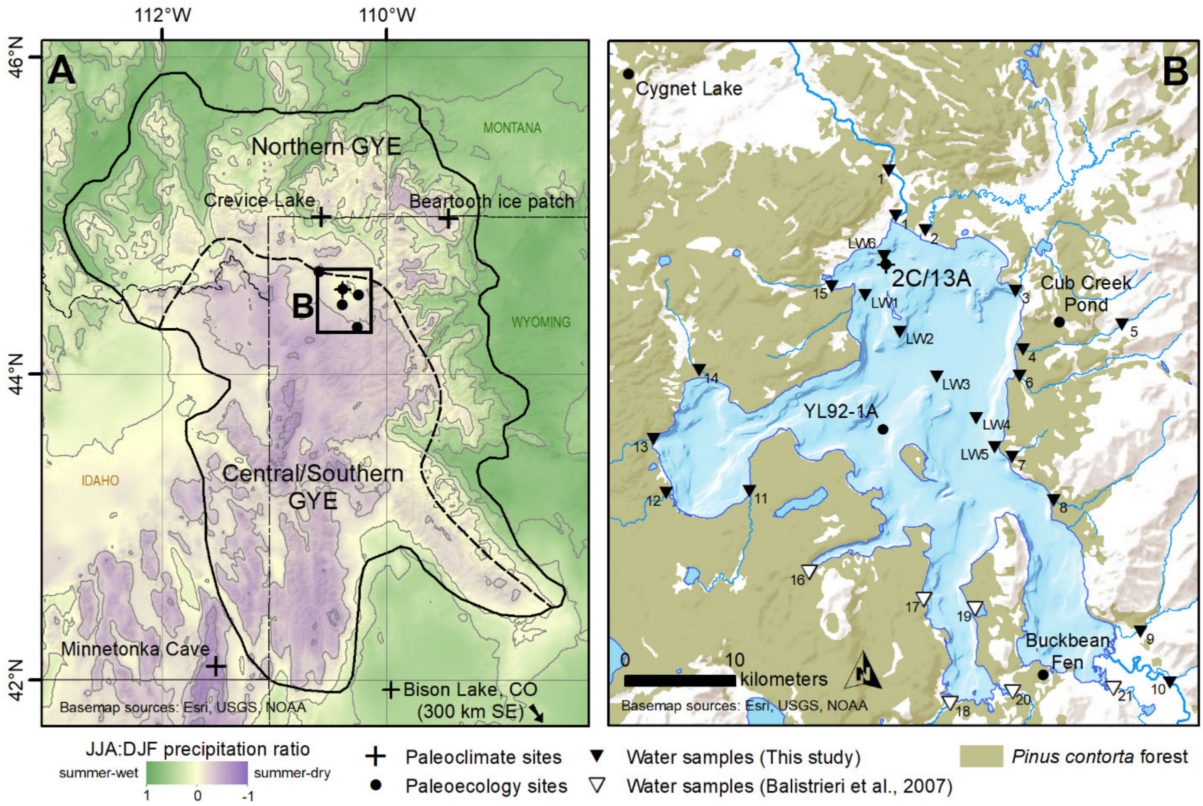

Figure 1: Panel A – Regional map of the Greater Yellowstone Ecosystem (GYE) (extent indicated by the solid black line) and regional paleoclimatic and paleoecologic records discussed in text. The precipitation regime (*sensu* Whitlock and Bartlein, 1993) is calculated as a standardized ratio of summer to winter precipitation (JJA:DJF) from PRISM climate data (PRISM Climate Group, 2004) and is the indicator used to differentiate the Central/Southern and Northern GYE, which are separated by a dashed line. A thin dot-dashed line represents the Wyoming state border. Paleoclimate sites are indiciated by a plus and paleoecology sites by a filled-in circle.
Panel B – Simplified bathymetric map of Yellowstone Lake based on data from Morgan et al., 2007a. The location of cores YL16-2C and YL16-13A are shown. Water samples taken in 2018 from the main tributaries surrounding the lake and surface lake waters (LW) are represented as hollow triangles. Water sample locations from Balistrieri et al. (2007) are shown as filled-in triangles.

This research builds on previous studies of the postglacial history of Yellowstone Lake, including its lake-level history (Meyer and Locke, 1986; Locke and Meyer, 1994; Pierce et al., 2007), sediment stratigraphy (Tiller, 1995), and the evolution of an endemic microalgae (Theriot et al., 2006). We add to this research by providing new high-resolution data from a suite of paleoenvironmental proxies, as well as the first water balance information based on $\delta^{18}O_{diatom}$ measurements, to deepen our knowledge of the Holocene evolution of the lake and its watershed. Specifically, the objective of our study is to address whether millennial- and submillennial-scale climate variations altered terrestrial and aquatic ecosystem conditions in a watershed with significant hydrothermal influence. To this end, new cores, collected from Yellowstone Lake in 2016, were examined to reconstruct changes in hydroclimate, using the oxygen isotope composition of diatom frustules ($\delta^{18}O_{diatom}$), changes in vegetation and fire history from pollen and charcoal data, and biological and physical changes in the lake from diatom and bulk geochemical records. We also compare the climate history of Yellowstone Lake region with other locations in the northern Rocky Mountains.

1.1 Site description

Yellowstone National Park, the core of the GYE, is located 600 km east of the Pacific Ocean and has a continental subarctic climate (Despain, 1987). The region is influenced in winter by Arctic and Pacific air masses and during summer by warm, moist air originating from the Gulf of Mexico and subtropical Pacific (Despain, 1987; Dirks and Martner, 1982). At Yellowstone Lake, precipitation is equally distributed throughout the year, peaking slightly in spring (yearly mean is 543±46 mm (1σ) from 1988 to 2018, NOAA dataset). Mean temperature is −10±1.4°C (1σ) in winter and +11.8±1.5°C (1σ) in summer (1988-2018, NOAA dataset).

Yellowstone Lake is typically dimictic, overturning in the spring and fall; the water column is thermally stratified in summer and winter, and the surface is frozen from mid-December/January to mid-May/June (Theriot et al., 2006). Nutrient and ionic concentrations of the lake are characteristic of alpine lakes (8.1 m Secchi depth, 200 µg/L total P, 0.2 mg L^{-1}

Kjeldahl-N, 86 μS/cm conductivity, 64 μeq L^{-1} total alkalinity) (Theriot et al., 1997; Kilham et al., 1996), and total dissolved solids (TDS) average 41.0 mg L^{-1} (Balistrieri et al., 2007; Gemery-Hill et al., 2007). The pH of deep water is circumneutral (6.9 in Mary Bay and 7.4 near Stevenson Island; Balistrieri et al., 2007), and the average pH of all water depths is 7.4±0.3 (1σ) (Theriot et al., 1997). The Yellowstone River is the primary tributary of Yellowstone Lake, and its inflow at the southern end of the Southeast Arm is ~70% of the lake's total annual water input (Fig. 1); more than 140 smaller tributaries also flow into the lake (Balistrieri et al., 2007). The Yellowstone River exits Yellowstone Lake at its northern margin and is the only outlet (Fig. 1).

Vegetation of the Yellowstone Lake watershed varies strongly with geology and elevation. Most of the Yellowstone Plateau to the north and west of Yellowstone Lake is underlain by rhyolitic lava flows (Christiansen, 2001) that produce nutrient-poor soils, and, as a result, the vegetation is dominated by closed *Pinus contorta* forest (Despain, 1990). On soils derived from andesitic or sedimentary nutrient-rich substrate to the south and east of Yellowstone Lake (Christiansen, 2001), the vegetation consists of mixed conifer (*Abies lasiocarpa*-*Picea engelmannii*-*Pinus contorta*-*Pinus albicaulis*) forest and meadows that support *Festuca idahoensis*, *Agropyron trachycaulum*, and a diverse suite of herbs (Despain, 1990). Steppe communities in Hayden and Pelican valleys, underlain by lake sediments of Pleistocene age (Richmond, 1977), are dominated by *Artemisia* (*A. cana* and *A. tridentata*) (Despain, 1990). Above ~2800 m elevation in the Absaroka Range, upper treeline is composed of *P. albicaulis* parkland or krummholz, and above ~2900 m elevation is tundra (Despain, 1990). The fire regime of the subalpine forests is characterized by large, infrequent, and high-severity fires (Turner et al., 1994; Schoennagel et al., 2003). Charcoal data from a *P. contorta* forest site located northwest of Yellowstone Lake (Cygnet Lake, Millspaugh et al., 2000) suggest 2–5 fire episodes/1000 years for the last two millennia, and data from a site in mixed-conifer parkland to the south (Trail Lake, Whitlock et al., 2003) indicate 6–13 fire episodes/1000 years over the same period (Millspaugh et al., 2000; Whitlock et al., 2003). Two large fire episodes occurred in recent centuries in the Yellowstone Lake watershed, the first ca. 1700 CE (1690-1710) and a second in 1988 CE (Romme and Despain, 1989).

1.2 Climate History

The GYE's postglacial climate history is the result of slow variations in the seasonal cycle of insolation and their impact on regional patterns of atmospheric circulation. These large-scale controls are modified by the region's topography, creating considerable spatial heterogeneity in temperature and precipitation. Central and Southern GYE, including Yellowstone Lake, is under the influence of the northeastern Pacific subtropical high-pressure system in summer, and this circulation feature was stronger in the early Holocene as a result of higher-than-present summer insolation, bringing warm dry conditions (Whitlock and Bartlein, 1993). In contrast, Northern GYE is relatively dry in winter and receives summer precipitation from moisture sources in the subtropical Pacific and Gulf of Mexico. During the early-Holocene summer insolation maximum, monsoonal circulation was enhanced relative to present day, bringing more summer precipitation and making the region warmer and wetter than present (Whitlock and Bartlein, 1993). Thus, two precipitation regimes presently exist in the GYE, and they have had different histories as a result of the two circulation patterns and their changes through time.

In Central and Southern GYE (a summer-dry area in that most of the precipitation is received in winter), existing paleoclimatic data indicate that overall conditions were warm and dry in the early Holocene and became progressive cooler and wetter as summer insolation declined and the subtropical high-pressure system weakened. In contrast, Northern GYE (the summer-wet area) was warm and relatively wet in the early Holocene and became cooler and more arid in recent millennia in response to the insolation forcing and attendant decline of summer monsoonal moisture (Whitlock and Bartlein, 1993).

2. Methods

An 11.62-m-long sediment core was retrieved with a Kullenberg sampler (Kelts et al., 1986) from 61 m water depth in northern Yellowstone Lake in September 2016 (44°32'21.2"N 110°23'20.4"W; Fig. 1; core YLAKE-YL16-2C-1K, referred to informally as core YL16-2C, of Morgan et al., 2021). An additional 0.54 m-long core was retrieved with a gravity corer from northern Yellowstone Lake in 2017 (44°30'38.9"N 110°21'21.9"W; Fig. 1; core YLAKE-YL17-13A-1G, referred to informally as YL17-13A) to recover the sediment-water interface. Cores were shipped to the LacCore facility at the University of Minnesota–Twin Cities for initial core description, physical property scanning, high-resolution photography, and subsampling. Magnetic susceptibility (MS) was measured using a Geotek MSCL-XYZ automated point-sensor split-core logger. The working half of cores were shipped to the Large Lake Observatory at the University of Minnesota-Duluth and scanned with an ITRAX X-ray Fluorescence Core Scanner. The long and short cores were correlated based on charcoal stratigraphy (see section 3.3 for details). All core depths hereafter refer to the composite record (YL16-2C and YL17-13A combined) unless otherwise indicated.

2.1 Age-depth Model

Thirteen samples including terrestrial plant remains, bulk sediment, and pollen concentrates were collected for accelerator mass spectrometry (AMS) radiocarbon dating (Table 1; Schiller et al., 2021). Additional age controls included the sediment-water interface from the gravity core (YL17-13A), a prominent charcoal peak attributed to a major fire episode ca. 1700 CE (Romme and Despain, 1989, see section 3.3 for details), and the 0.5-cm-thick Mazama ash, identified chemically with electron microprobe analysis (Schiller et al., 2020). Relative to the uncertainty of the age-depth model, neither the ash nor a siliciclastic unit, interpreted as a thin (7 cm) hydrothermal explosion deposit (Morgan et al., 2021), were thick enough to justify removal from the composite depth of the age model. Radiometric dates were converted to calendar ages with the IntCal13 calibration curve (Reimer et al., 2013) and modelled against depth using the software package Bacon (Blaauw and Christen, 2011) (Table 1). Assignment of the mean sediment accumulation rate was set to 10 yr cm^{-1}, as suggested by the program Bacon and closely matching our data. This rate is similar to Holocene sediment accumulation rates estimated for other locations within Yellowstone Lake (~15 yr cm^{-1}, Tiller, 1995; 17-10 yr cm^{-1}, Johnson et al., 2003; ~15 yr cm^{-1}, Theriot et al., 2006). Thickness for spline calculation was set at 20 cm, above which the model diverged greatly from the age controls provided.

Table 1: Yellowstone Lake composite core age controls

Accession No.	Composite core Depth (cm)	Material Dated[1]	Age ^{14}C	$\delta^{13}C$ ‰ VPDB	2σ cal age range[2]	Source
	0	sediment-water interface (13A)			-67	

	12	1700 CE fire			240–260	Romme and Despain (1989)
OS-135957	328	t. plant remains	2590±20	-26.33	2723–2754	
OS-135958	402	t. plant remains	3150±25	-27.97	3272–3285, 3339–3445	
OS-136956	624	t. plant remains	4510±20		5053–5190, 5213–5296	
	951	Mazama ash			7584–7682	Egan et al. (2015)

[1] t. plant remains (terrestrial plant remains) including wood

[2] Calibrated ranges calculated by CALIB (version 7.1, Stuiver et al., 2019)

2.2 Biogenic silica (BSi), Total Organic Carbon (TOC), and C/N Ratios

Biogenic silica (SiO_2) concentrations (BSi) were analyzed on freeze-dried, homogenized samples using sequential alkaline extraction (Conley and Schelske, 2001) at 8-cm sampling intervals. The contribution of mineral dissolution on extraction of SiO_2 from sediments was small relative to the amount of SiO_2 extracted, so mean values were used to estimate BSi concentrations with no mineral correction applied. The extracted dissolved silicon was quantified using the automated molybdate-blue method (Strickland and Parsons, 1972), with a Smartchem 200 AMS discrete analyzer with an instrumental error of ±3.7%. The same freeze-dried homogenized samples (40-cm sampling interval) were analyzed for total organic carbon (TOC) and total nitrogen (TN) content using an elemental analyzer (COSTECH ECS4010) with a mean analytical uncertainty of ±0.3wt% (1σ) for TOC. Samples were treated with 500 μL of 2M HCl to remove any $CaCO_3$ and then packed in silver and tin capsules for TOC and TN analysis. The sedimentary BSi and TOC fluxes were calculated as follows (Ragueneau et al., 2001):

$$BSi_{flux}\ [g \cdot cm^{-2} \cdot yr^{-1}] = (1-\phi) \cdot SR \cdot \rho \cdot BSi \text{ or}$$

$$TOC_{flux}\ [g \cdot cm^{-2} \cdot yr^{-1}] = (1-\phi) \cdot SR \cdot \rho \cdot TOC$$

where ϕ is the sediment porosity, SR is the sedimentation rate (cm yr^{-1}), and $\boldsymbol{\rho}$ is the bulk wet-sediment density. Bulk wet-sediment density (g cm^{-3}) is taken from the Geotek MSCL-S whole core scans. The sediment porosity is estimated as the average particle density based on the sum of the percentages of particle densities of BSi (2.00 g cm^{-3}) (DeMaster, 2003), TOC (1.25 g cm^{-3}), and the mineral content (2.65 g cm^{-3}) (Boyd, 2012). Mineral content was calculated by difference assuming diatoms as BSi and organic carbon as TOC are the only significant non-mineral (or glass) phases. Detrital minerals in Yellowstone Lake sediments were determined by SEM (scanning electron microscope) observations with semi-quantitative EDS (energy dispersive XRF) analysis and semi-quantitative XRD (X-ray diffraction) analysis (Shanks et al., 2007, Morgan et al., 2021).

2.3 Pollen & Charcoal

Subsamples of 1 cm^3 at 1- to 24-cm intervals were prepared for pollen analysis following standard procedures (Bennett and Willis, 2001). Due to the large lake surface area and inflow of the Yellowstone River and other tributaries, the pollen source area is assumed to be large, and the pollen record describes vegetation history at a regional scale (Jacobson and Bradshaw, 1981; Sugita, 1993). Constrained cluster analysis (CONISS) was conducted to identify pollen zones. The record described here augments a close-interval pollen study of Schiller et al. (2020), which focused on changes immediately before and after the deposition of the Mazama ash, and an earlier lower resolution pollen record from the central part of the lake (Theriot et al., 2006).

Continuous subsamples (~2 cm^3) were collected for charcoal analysis at 1-cm increments from the entire composite core, providing a high-resolution analysis of past fire activity. Charcoal particles >125 μm in diameter were analyzed, as this size fraction registers local fire episodes (Whitlock and Millspaugh, 1996). The charcoal record was separated into two components: a long-term trend, which represents slow variations in regional charcoal production, charcoal redeposition, and sediment mixing (Whitlock and Larsen, 2001); and peaks, which are inferred to represent fire episodes (one or more fires during the time span of the charcoal peak) (Whitlock and Millspaugh, 1996; Higuera et al., 2011). To accomplish this decomposition, we used CharAnalysis software (Higuera et al., 2009) to analyze charcoal accumulation rates (CHAR, particles cm^{-2} yr^{-1}). Millspaugh and Whitlock (1995) found that a core in the West Thumb basin of Yellowstone Lake only recorded the very large 1988 CE fires, without documenting smaller ones. Therefore, given the typically high-severity of most fires burning in the *Pinus contorta*-dominated forests today (Despain, 1990; Anderson and Romme, 1991; Turner et al., 1999), peaks in our composite core are interpreted as very large fire episodes.

2.4 Fossil diatoms

Subsamples (~0.5 cm^3) for diatom analysis were collected every 4 cm through the core and were processed and analyzed using standard methods (Battarbee, 2003). Diatom valves were identified at 1000× magnification using a Leica DM2500 transmitted light microscope fitted with differential interference contrast (DIC) and equipped with a 5-Megapixel camera or a Leica DMRX fitted with phase contrast. Diatom species were identified, including habitat preference, using diverse taxonomic resources relevant to the northern Rocky Mountains (e.g., Bahls, 2005; Spaulding and Edlund, 2019). Constrained cluster analysis (CONISS) was conducted on species-assemblage percentage data using the Rioja R package (Juggins, 2017) to identify diatom zones. The ratio of plankton:tychoplankton and benthon (P:T and B) percentages was calculated to infer broad changes in diatom habitat as determined from the input of pelagic (plankton) versus attached (tychoplankton and benthon) diatom species to the coring site.

2.5 Isotopes in diatoms ($\delta^{18}O_{diatom}$) and water samples (δD_{lake}, $\delta^{18}O_{lake}$)

Subsamples (~2 cm^3) for diatom isotope analysis were collected from every 8 cm of the core. Samples were prepared for isotope analysis following several cleaning steps to remove contaminants (Morley et al., 2004). Finally, samples were cleaned in 0.05 M sodium pyrophosphate ($Na_4P_2O_7$) and sieved at 25 µm to isolate *Stephanodiscus yellowstonensis*, thereby reducing potential biases due to different species' vital effects (Swann et al., 2007). The purity of samples was checked using a scanning electron microscope (Tescan Mira3 High Resolution Schottky FE-SEM) (see picture in Supplementary Material 1). Oxygen isotope analysis was performed at the National Environmental Isotope Facility, British Geological Survey (UK), using stepwise fluorination (Leng and Sloane, 2008), and the sample was converted to CO_2 through reaction with heated graphite (Clayton and Mayeda, 1963) and analyzed on a Thermo Finnigan MAT 253 dual inlet mass spectrometer. Oxygen isotope values are reported in standard delta notation ($\delta^{18}O_{diatom}$) as per mil (‰). Analytical reproducibility of laboratory working standards was <0.14‰ (n=18: 1σ) and <0.2‰ for samples based on 21 replicates.

Water samples from Yellowstone Lake (n=6) and tributaries (n=17) were collected in the summer of 2018 to determine the major factors influencing δD and $\delta^{18}O$ in lake waters (see locations on Fig. 1 and geographic coordinates in Supplementary Material 2). Oxygen isotope ($\delta^{18}O$) measurements were made at the British Geological Survey using the CO_2 equilibration method with an Isoprime 100 mass spectrometer plus Aquaprep device. Deuterium isotope (δD) was measured using an online Cr reduction method with a EuroPyrOH-3110 system coupled to an GVI IsoPrime mass spectrometer (Morrison et al., 2001). Isotope measurements used internal standards calibrated against the international standards VSMOW2 and VSLAP2. Errors (1σ) are typically ±0.05‰ for $\delta^{18}O$ and ±1.0‰ for δD.

3. Results

3.1 Age-depth model

The age-depth model (Fig. 2) (the "Terrestrial Plant Remains" model of Schiller et al., 2021) was based on three calibrated macrofossil radiocarbon ages, the Mazama ash (Egan et al., 2015), the sediment-water interface, and a peak in charcoal attributed to widespread fire in ca. 1700 CE (Romme and Despain, 1989) (Table 1). Bulk sediment and pollen concentrates collected for AMS dating were rejected as erroneously old due to probable contamination of reworked pollen or dead carbon from degassed magmatic or pre-Tertiary basement sources (Schiller et al., 2021). Failure of bulk sediment and pollen concentrate dates (Schiller et al., 2021) and the paucity of any other suitable terrestrial material prevented further improvement of the age model. The resultant model has wide error ranges (200–1000 cal years) between age controls and of up to 2200 cal years where ages were extrapolated at the bottom of the core. Point age estimates from the composite core would be aptly treated with caution by the reader. The model produced an extrapolated basal age of ca. 9880 cal yr BP. The *Pinus*-dominated pollen spectra at 1162 cm depth in core YL16-2C (9880 cal yr BP) are consistent with a Holocene age for the record (Whitlock, 1993; Iglesias et al., 2018). The average sediment accumulation rate for the core was calculated to be 8.4 years cm^{-1}, or a sedimentation rate of 0.12 cm yr^{-1}.

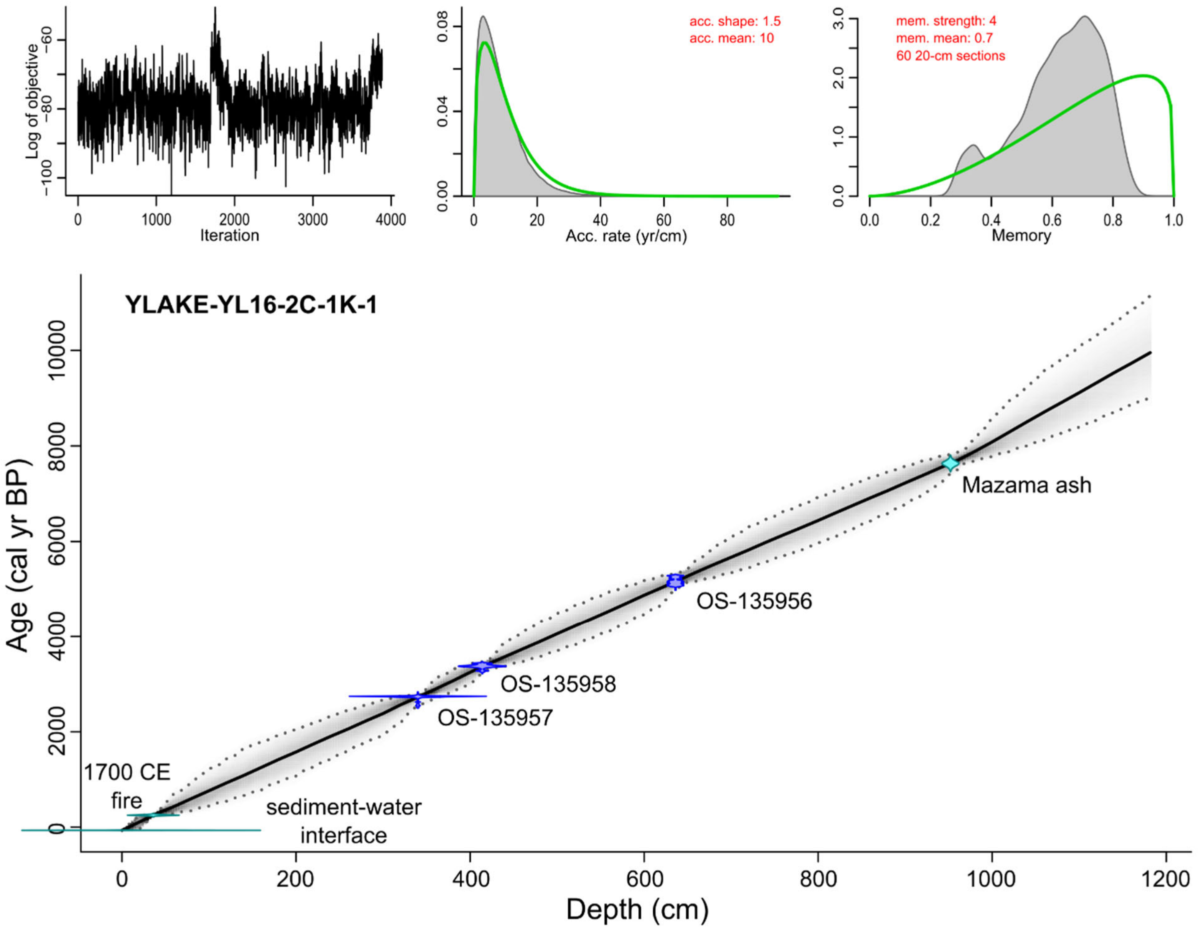

Figure 2: Age-depth model for Yellowstone Lake composite core. Dark line is the mean probability age from all age-depth iterations, representing the best point estimate of age for any given depth. Gray cloud represents age model probability and contains a 95% confidence interval (dashed lines). Iteration history (left inset), prior and posterior densities of the mean accumulation rate (middle inset), and prior and posterior of the memory (right inset).

3.2 Lithology, BSi, TOC, & C/N Ratios

The lithology was divided into eight limnic facies (units) modified after Tiller (1995) (Table 2; Fig. 3). Starting at the top of the core, units IX, VIII, VII, and VI are brown diatomaceous muds, weakly laminated, with black sulfidic layers. Unit VI has moderately developed laminae of 0.5 cm thickness. Unit V is laminated diatomaceous mud, whereas unit IV is uniformly well-laminated brown and black diatomaceous mud. Units III and IIb are classified as diatomaceous mud, whereas unit IIb is laminated to weakly laminated (Morgan et al., 2021).

Table 2: Lithological units in core YL16-2C (presented with composited core depth) and described in Morgan et al., (2021), together with biogenic silica (BSi) and Total Organic Carbon (TOC) data from this study.

Lithological unit	Description	Sedimentation regime	Depth (m)
IX	olive-gray diatomaceous mud, high TOC (2.9 to 3.3%), lower BSi from 25 to 36%, decreasing BSi flux from 9.1 to 3.6 mg $SiO_2/cm^2/yr$	column instability and turbulence	20–71
VIII	weakly diatom-laminated, olive-gray diatomaceous mud, high TOC (2.5 to 3.2%), high BSi from 30 to 45%, high BSi flux from 3.2 to 12.2 mg $SiO_2/cm^2/yr$	moderate bioturbation, calm sedimentation with high aquatic production	71–373
VII	weakly, diatom-laminated, olive-gray diatomaceous mud, high TOC (2.1 to 2.6%), high BSi from 29 to 38%, slightly increasing BSi flux towards top from 6.5 to 12.1 mg $SiO_2/cm^2/yr$	calm sedimentation with high aquatic production	
VI	intermediately banded, olive-gray diatomaceous mud, moderate TOC (1.8 to 2.9%), fluctuating BSi from 25 to 48%, regularly fluctuating BSi flux from 2.5 to 12.9 mg $SiO_2/cm^2/yr$	water column instability, regular mixing resulting in laminated sediment, calm sedimentation, great oxygenation of bottom water	373–848

V	Interbedded, diatom-laminated olive-gray diatomaceous mud, moderate TOC (1.5 to 2.4%), fluctuating BSi from 28 to 50%, high BSi flux from 1.8 to 19.7 $SiO_2/cm^2/yr$ with slightly increasing trend after deposition of hydrothermal explosion breccia (9.7 m)	turbulent water column, high BSi production, heavily silicified population of diatoms, oxygenated bottom water	848–1048
IV	well-diatom-laminated, olive-gray diatomaceous mud, low TOC (1.7 to 1.9%), stable high BSi from 31 to 43%, increasing BSi flux from 5.1 to 12.2 mg $SiO_2/cm^2/yr$	stable water column, increasing diatom productivity, low bottom water oxygenation	1048–1122
III	olive-gray, diatomaceous mud with sandy oxides, sulfides replaced by oxide concretions, plant detritus, higher TOC (2.1%), lower BSi from 26 to 36%, variable BSi flux from 4.8 to 10.8 mg $SiO_2/cm^2/yr$	stable water column conditions, high diatom productivity, low bottom water oxygenation, sulfur reduction, low bioturbation	1122–1165
IIb	occasionally sulfide-or-diatom laminated mud, low TOC (1.8%), moderate BSi concentration of 34%, lower BSi flux of 4.5 mg $SiO_2/cm^2/yr$	stable water column, with high diatom productivity and low bottom water oxygenation	1165–1182

A simplified lithologic log (Fig. 3) includes titanium (Ti) values as an indicator of detrital input, mass accumulation rate (MAR), total organic carbon (TOC) content and flux, C/N ratios, biogenic silica (BSi) content (wt% SiO_2), and BSi flux. Mineral content (mean 61 dry wt%, 1σ = 6 wt%, n=150) and BSi content (mean 36 dry wt%, 1σ=6 dry wt%, n=150) dominated the sediment composition, with a minor component of TOC (mean 2.3 dry wt%, 1σ=0.5 wt%, n=27).

The BSi flux is mainly driven by changes in MAR and shows generally stable BSi accumulation of 8.0 mg SiO_2 $cm^{-2}yr^{-1}$ (1σ=2.8 mg SiO_2 $cm^{-2}yr^{-1}$) throughout the record.

Detrital minerals, based on XRD and SEM analyses, were composed of (a) major minerals, including alkali and plagioclase feldspars, rhyolitic rock fragments, pyroxene, and quartz; (b) minor minerals (e.g., ilmenite, titano-magnetite, apatite, pyrite, anhydrite); and (c) trace minerals (clays) (Morgan et al., 2021; Shanks et al., 2007; 2019). TOC wt% and C/N ratios (6.8–10.9) increased modestly up-core (Fig. 3).

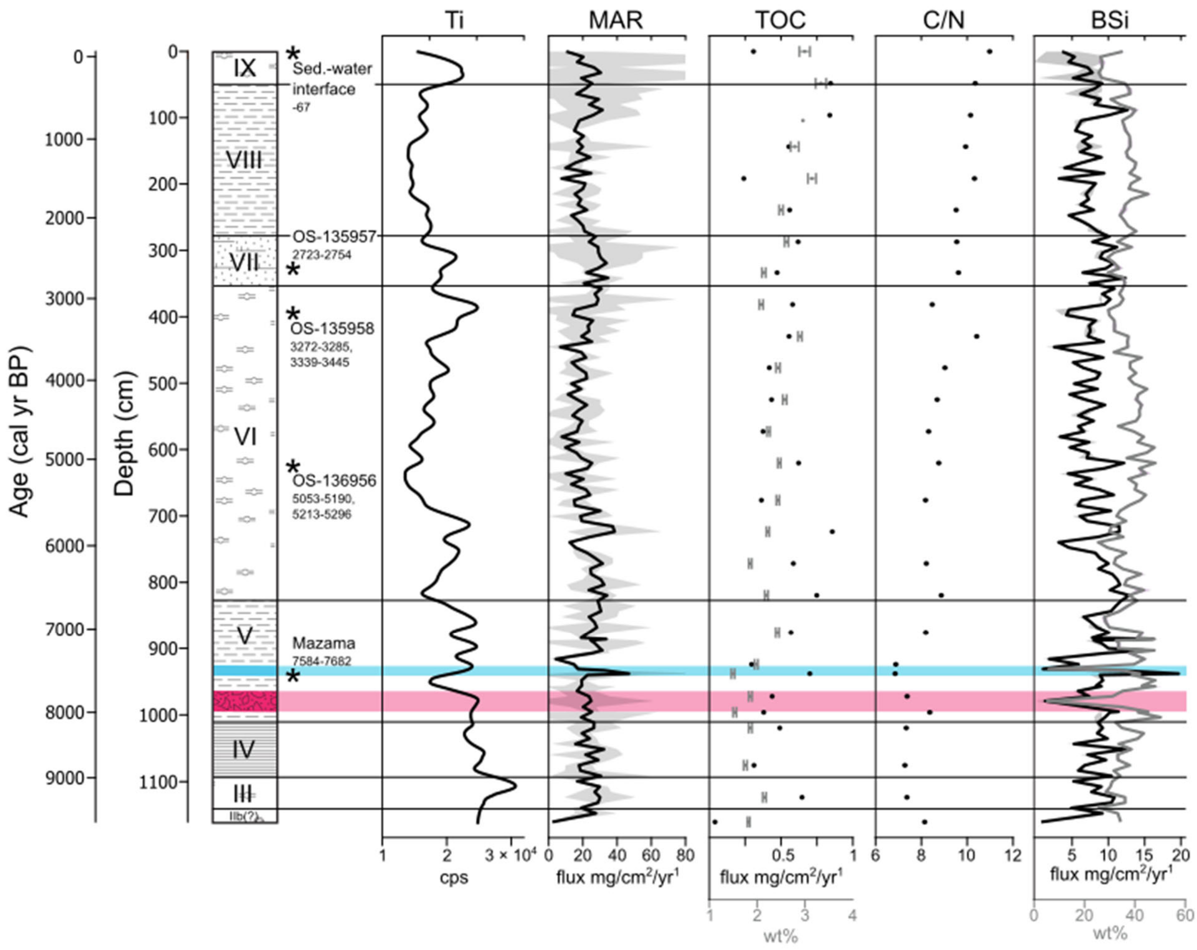

Figure 3: Lithological units identified in Core YL16-2C refer to units characterized in Table 2, and contacts are shown as solid black horizontal lines. Age controls are indicated (*), with 2σ calibrated age range. Lithological descriptions are supported by XRF data – titanium (Ti) as a detrital input proxy. The sediment mass accumulation rate (MAR) is presented with uncertainties

propagated from the age-depth model, shown as shading. Total organic carbon (TOC) shown in gray with 1σ error bar and calculated carbon flux in black. The C/N ratio is represented by black points. Biogenic silica (BSi) (gray line) is expressed as dry sediment wt% SiO_2 with 1σ shading in gray. The BSi flux (black line) is presented with the uncertainties propagated from the age-depth model as shading in gray. The widths of the blue and pink lines representing the 0.5-cm-thick Mazama ash and the 7-cm-thick hydrothermal explosion deposit in core YL16-2C, respectively, are exaggerated in this diagram for purposes of illustration.

BSi concentration varied greatly at the base of the core (1170–820 cm depth) (25.7–50.2 wt% SiO_2, 1σ=±6.0 wt%, n=48), as did BSi flux (0.75–19.7 mg cm^{-2} yr^{-1}). The middle part of the core (820–350 cm depth) had relatively high BSi concentrations (25–48 wt% SiO_2, 1σ=5.0 wt%, n=59) and variations in BSi flux from 2.48 to 12.15 mg cm^{-2} yr^{-1}. The top of the core (350–0 cm depth) had slightly lower BSi concentrations (25–45 wt% SiO_2, 1σ=4.5 wt%, n=43), with BSi flux from 3.22 to 12.25 mg cm^{-2} yr^{-1}).

3.3 Pollen and charcoal

Pollen and charcoal data were divided into two zones based on CONISS results of the terrestrial pollen percentages. Zone YL-P1 (1174–740 cm depth; 9880–6000 cal yr BP) was dominated by *Pinus* (55–77%), except immediately above the Mazama ash where *Pinus* values declined to 48%. Most identifiable *Pinus* grains were *P. contorta*-type, with low to moderate amounts of *P. albicaulis*-type (2–36% of total *Pinus*). *Picea* (<4%), *Abies* (<3%), *Pseudotsuga* (<2%), *Juniperus*-type (<3%), and *Salix* (<2%) were present in small proportions. Shrub and herbaceous steppe taxa, including *Artemisia* (10–24%), Poaceae (<4%), and Amaranthaceae (<8%) constituted another major component, along with trace (<1%) abundance of extra-local xerophytic pollen types, including *Sarcobatus* and *Ephedra viridis*-type. CHAR (mean 0.3

particles cm^{-2} yr^{-1}) was generally steady. Fire frequency (2.5 episodes 1000 years^{-1}) and peak magnitude (mean peak magnitude 6.8 particles cm^{-2} yr^{-1}) were generally low (Fig. 4).

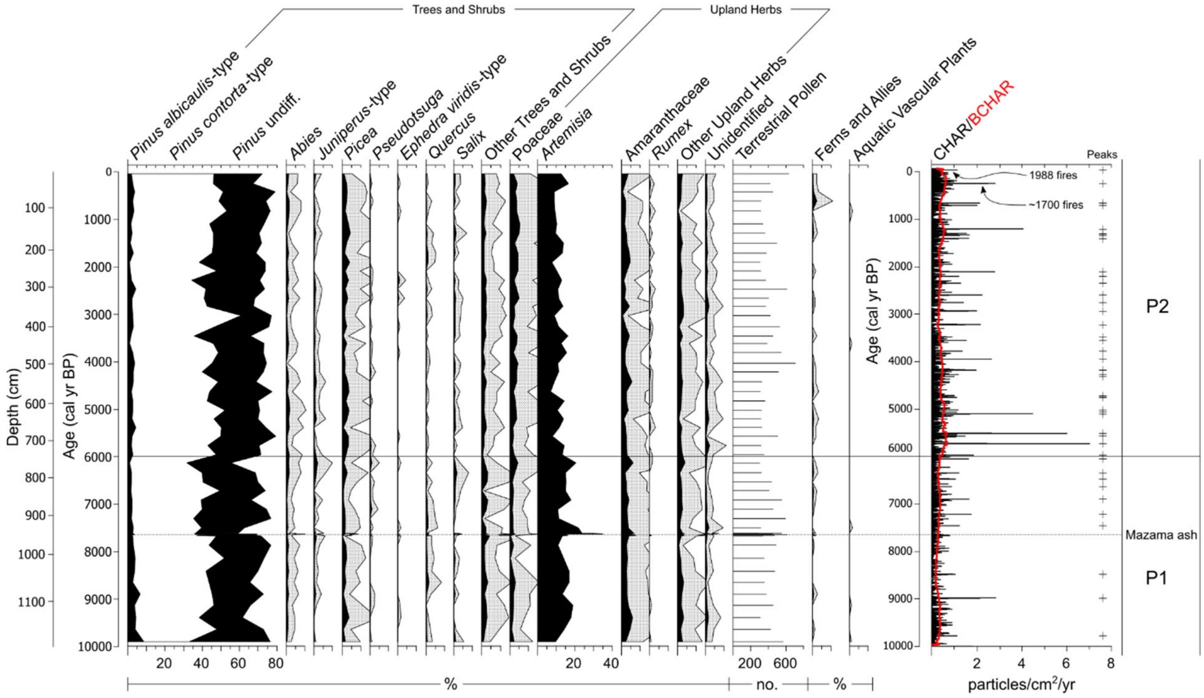

Figure 4: Stratigraphic plot of important pollen types and CHAR from the composite core plotted by age. Gray pollen plots show 5x exaggeration.

Zone YL-P2 (740–0 cm depth; 6000–-67 cal yr BP) was characterized by slightly higher percentages of *Pinus* (66–79%) and a lower proportion of *P. albicaulis*-type (2–11% of total *Pinus*) than Zone YL-P1. Other tree taxa were present in low percentages, including *Picea* (<5%), *Abies* (<3%), *Pseudotsuga* (<1%), *Juniperus*-type (<2%), and *Salix* (<2%). Steppe taxa, including *Artemisia* (7–16%) and Amaranthaceae (<6%), decreased in abundance. Poaceae percentages (<5%) increased somewhat, and *Rumex* was consistently detected in trace amounts (<1%). CHAR (0.4 particles cm^{-2} yr^{-1}) was slightly higher than Zone YL-P1. Large fire episodes were more frequent (5.0 episodes per 1000 years), and peak magnitudes were higher than before (mean peak magnitude 12.6 particles cm^{-2} yr^{-1}) (Fig. 4).

A distinct charcoal peak was present in the Kullenberg core (YL16-2C) at 24 cm depth and the gravity core (YL17-13A) at 36 cm depth, with charcoal concentrations of 37 and 39 particles cm^{-3}, respectively. Dendrochronological and charcoal data suggest only two large fire episodes in the last few centuries in the region, the 1988 CE fires and ca. 1700 CE fires (Romme and Despain, 1989; Higuera et al., 2011). This charcoal peak was too deep to be attributed to the 1988 fires; an overlying peak was evident in the YL16-13A gravity core at 3 cm depth, which we assign to the 1988 fires. The charcoal peaks at 24 cm depth in the Kullenberg core YL16-2C and at 36 cm depth in the YL17-13A gravity core are attributed to the ca. 1700 CE fire episode and used for stratigraphic correlation as noted previously.

3.4 Fossil Diatoms

The Yellowstone Lake diatom assemblage (>5% abundance) was composed of four planktic species (*Stephanodiscus minutulus, Aulacoseira subarctica, Asterionella formosa*, and *Stephanodiscus yellowstonensis*) and one tychoplanktic species complex (fragilaroids). CONISS results were used to group the percent abundance data into three major zones (Fig. 5).

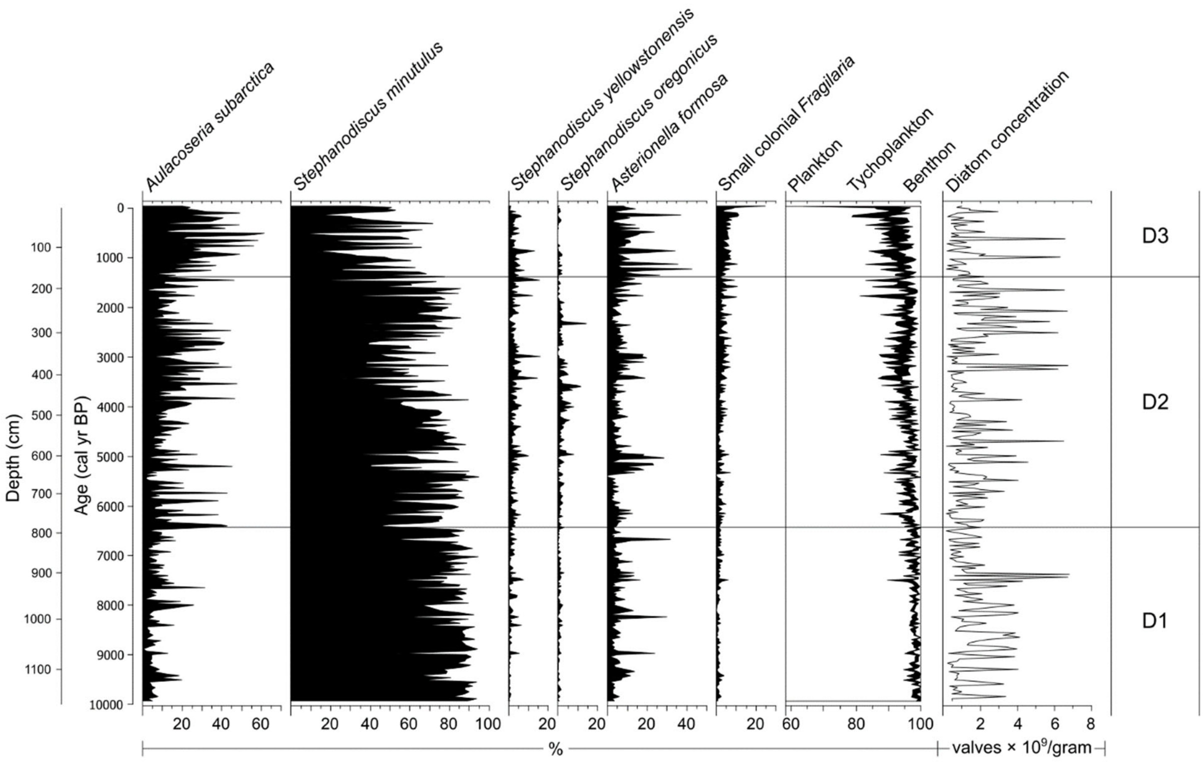

Figure 5: Stratigraphic plot of the composite core of abundant (>5%) diatom species, plankton (left-hand white shaded area):tychoplankton (black curve):benthon ratio (right-hand with shaded area), log-transformed diatom concentration (valves/gram) plotted by age and depth, and diatom zone (D1, D2, D3).

Zone YL-D1 (1174–793.5 cm depth; 9880–6430 cal yr BP) was dominated by *Stephanodiscus minutulus* (>50%), sometimes >90%. Short intervals with peaks in relative abundance of *Aulacoseira subarctica* (<35%) and *Asterionella formosa* (<40%) corresponded with decreases in *S. minutulus*. This zone routinely had high percentages of plankton and very low combined abundance (<5%) of tychoplanktic and benthic taxa compared to other zones. *Stephanodiscus yellowstonensis* and *Stephanodiscus oregonicus* were at their lowest abundance (<2%) in zone YL-D1.

Zone YL-D2 (793.5–179.5 cm depth; 6430–1380 cal yr BP) also was dominated by *Stephanodiscus minutulus* (30–90%), but with greater variability in abundance than YL-D1, primarily driven by changes in relative abundances of *Aulacoseira subarctica* (5–50%) and

Asterionella formosa (5–30%). In addition, *Stephanodiscus yellowstonensis* (<15%), *Stephanodiscus oregonicus* (<15%), and small fragilaroids (<10%) were generally higher in relative abundance than in YL-D1. Although plankton still dominated the assemblage (80–95%), tychoplankton and benthon percentages (<7.5%) began to increase.

Zone YL-D3 (179.5–12.5 cm depth; 1380–57 cal yr BP) continued to be dominated by *Aulacoseira subarctica* (5–60%), *Stephanodiscus minutulus* (5–80%), and *Asterionella formosa* (2–40%), in addition to moderate *Stephanodiscus yellowstonensis* (<20%), low *Stephanodiscus oregonicus* (<2%), and higher small colonial fragilaroids than previous zones. Consistently higher relative abundances of *A. subarctica* and *A. formosa*, as well as a higher proportion of tychoplankton and benthon, make this zone distinctive.

3.5 Isotopes in diatoms ($\delta^{18}O_{diatom}$) and water samples (δD_{lake}, $\delta^{18}O_{lake}$)

Measurements of modern $\delta^{18}O_{lake}$ and δD_{lake} (‰, VSMOW2) are presented in Supplementary Material 2 and plotted on Fig. 6A, together with measurements of water samples taken in 1998/1999 (Balistrieri et al., 2007). Water samples from the tributaries plot on or near the global meteoric water line, whereas lake-water samples fall on a local evaporation line. In August 2018, mean $\delta^{18}O$ in the main tributaries entering the lake was -18.0 ‰ and at the Yellowstone River inlet was -18.6 ‰. Lake-surface water in 2018 from different locations had mean $\delta^{18}O_{lake}$ of -15.7 ‰, and mean $\delta^{18}O$ at the Yellowstone River outlet was −15.9 ‰; both are slightly higher than values measured in 1998-1999. $\delta^{18}O_{lake}$ values in surface waters of the Southeast Arm were lower, consistent with inflowing Yellowstone River waters that had $\delta^{18}O_{lake}$ of -19.6 to -18.0 ‰ in samples collected in 1998 and 1999 (Balistrieri et al., 2007) and of -18.6

‰ in 2018. A snow sample taken at Cub Creek during fieldwork in 2018 had a $\delta^{18}O_{snow}$ value of −24.8 ‰ (Fig. 6A; 6B).

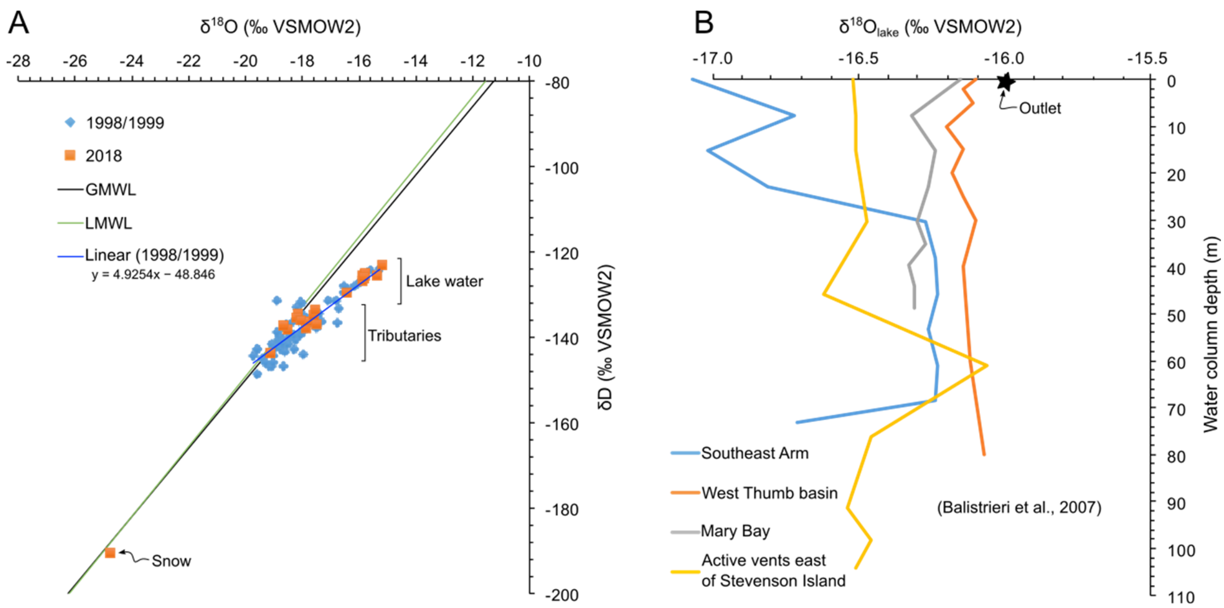

Figure 6: (A) $\delta^{18}O$ and δD (‰ VSMOW2) in water samples from snow, tributaries entering the lake, and lake surface taken during summer 2018 in orange and compared to measurements performed in 1998/1999 in blue, published in Balistrieri et al., 2007. GMWL: Global Meteoric Water Line from Craig, 1961. LMWL: Local Meteoric Water Line (Kharaka and White, 2002). Linear: linear regression on water samples from 1998/1999. Locations, sampling dates, and sample values are presented in Supp. Material 2. (B) $\delta^{18}O$ (‰ VSMOW) according to depths from water columns of the Southeast Arm, West Thumb basin, Mary Bay, and in the active vent area east of Stevenson Island published in Balistrieri et al., 2007. Mean $\delta^{18}O$ value at the outlet is shown as a black star.

Average $\delta^{18}O_{diatom}$ (Fig. 7) for the entire record was +25.8 ‰ (VSMOW, 1σ= 0.66‰, n=112), with a minimum value of +24.2‰ at 661.5 cm depth (5380 cal yr BP) and a maximum value of +27.1‰ at 1064.5 cm depth (8830 cal yr BP). Thus, the range of variability was about +2.9‰. The $\delta^{18}O_{diatom}$ data clustered into two main zones: YL-O1 (1174–784 cm depth, 9930–6350 cal yr BP) and YL-O2 (784–12.5 cm depth, 6350–50 cal yr BP YL-O1 began with high $\delta^{18}O_{diatom}$, and values subsequently declined through the zone. Peaks at 1159.5, 1079.5, 1031.5, and 976.5 cm depth were the highest values of the record. YL-O2 had generally lower $\delta^{18}O_{diatom}$ than the previous zone. The first half of Zone YL-O2 (784–514 cm depth, 6350–4210 cal yr BP) was characterized by high variability in $\delta^{18}O_{diatom}$. Average $\delta^{18}O_{diatom}$ was +25.5‰ (1σ=0.22‰, n=25), with a peak at 743.5 cm depth (6030 cal yr BP), followed by a decreasing trend. $\delta^{18}O_{diatom}$ then increased after 564 cm depth (4600 cal yr BP). The second half of the Zone YL-O2 (514–354 cm depth, 4210–2910 cal yr BP) had higher $\delta^{18}O_{diatom}$, with two peaks at 436.5 and 404.5 cm depth (3310–3570 cal yr BP). During the late Holocene (354–177 cm depth, 2910–1440 cal yr BP), lower values were stable, with an average of +25.3‰ (1σ=0.06‰, n=15), and the most recent portion (177–12.5 cm depth, 1440–50 cal yr BP) had a peak in $\delta^{18}O_{diatom}$ with two samples at +26.1‰ (1σ=0.05‰).

4. Discussion

The results of our multi-proxy analysis of our Yellowstone Lake sediment core are discussed in three sections. First, in Section 4.1, we discuss the rationale for the interpretation of our individual proxies, particularly the lithologic and limnobiotic records. Then, in section 4.2, we reconstruct paleoclimate for the Yellowstone Lake basin through interpretation of our datasets. This section is divided into three subsections based upon major transitions in the proxy data: – early Holocene (9880–6700 cal yr BP), middle Holocene (6700–3000 cal yr BP), and late Holocene (3000–-67 cal yr BP). Within each subsection, we first reconstruct regional-scale hydroclimatic ($\delta^{18}O_{lake}$), followed by a discussion of basin-scale terrestrial (pollen/charcoal) and limnologic (diatoms/geochemistry) responses to climate change (Fig. 7). Finally, in section 4.3, we compare the hydroclimatic reconstruction at Yellowstone Lake to regional records within the northern Rocky Mountains (Fig. 8).

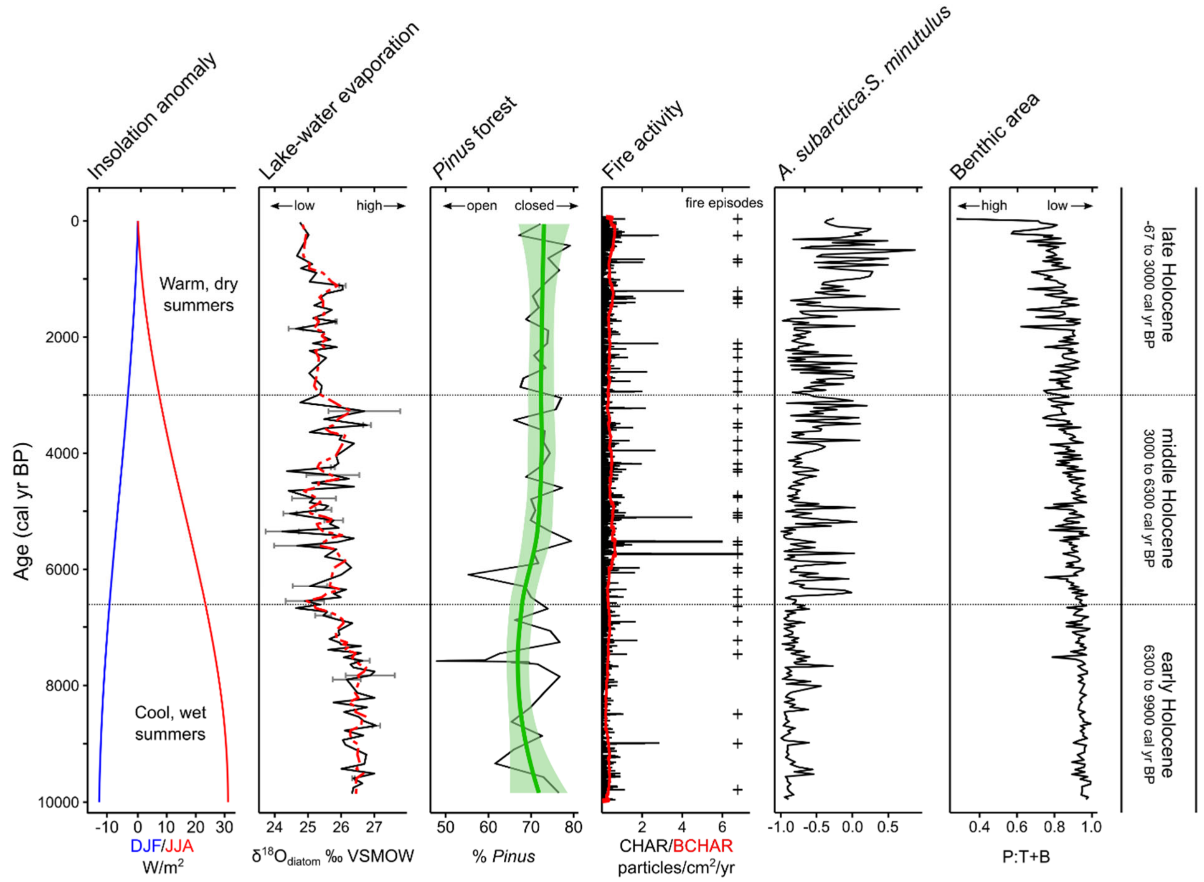

Figure 7: Summary of Holocene environmental proxy data for the Yellowstone Lake region plotted against summer insolation anomalies (data from Laskar et al., 2004, 44.5°N solution) for the composite core YL16-2C record. Oxygen isotope values from diatoms ($\delta^{18}O$) are expressed using a 3-point-moving-average line in red and error bars representing 1σ in gray. *Pinus* forest cover in the region is represented by % *Pinus* grains from Yellowstone Lake with an added lowess smoother (green with shaded standard deviation) to emphasize long-term trends. Fire activity is shown by Yellowstone Lake CHAR (black), BCHAR (red), and peaks (fire episodes, +). The ratio of *Aulacoseira subarctica:Stephanodiscus minutulus,* which represents variation in the duration of spring mixing (AF=long, SM=short). The inferred amount of benthic habitat is indicated by Planktonic:Tychoplanktonic+Benthic ratios, with higher values representing periods with less shallow-water habitat.

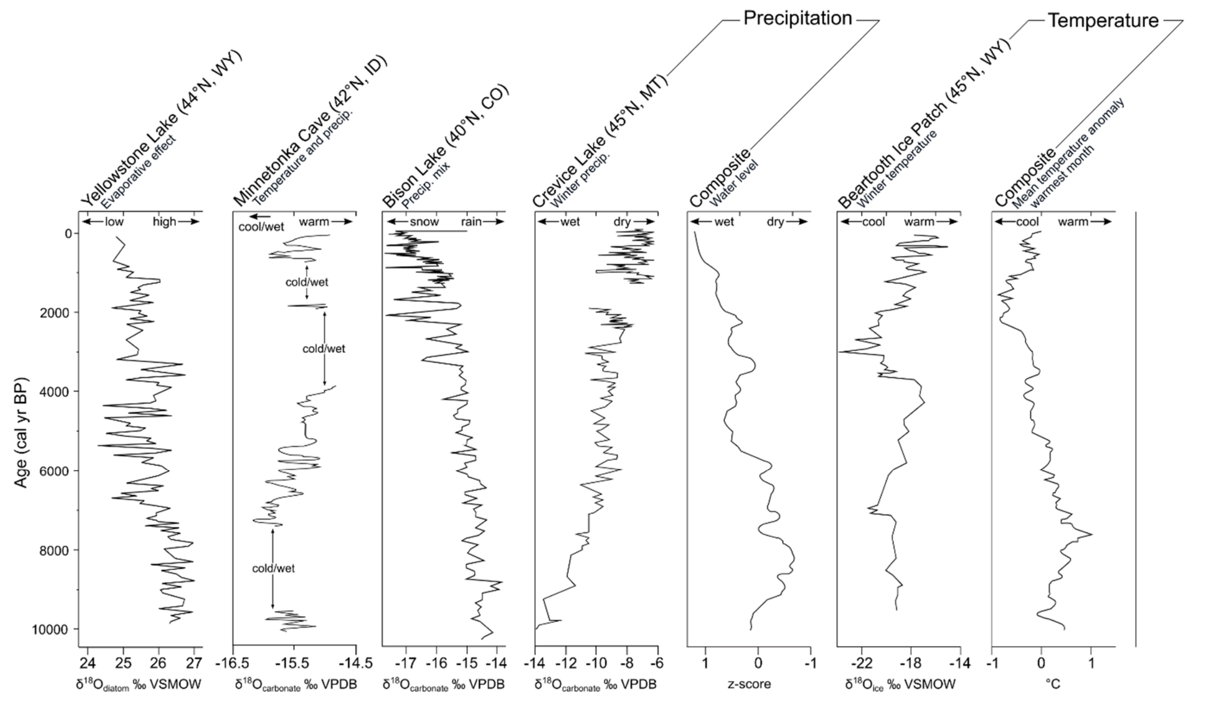

Figure 8: Paleoclimatic records from the central Rocky Mountains and surrounding regions according to ages, from left to right: $\delta^{18}O$ record (‰ VSMOW) at Yellowstone Lake (44°N) from diatoms (this study); $\delta^{18}O$ record on endogenic carbonates (‰ VPDB) at Bison Lake (40°N) in northern Colorado (Anderson, 2011); $\delta^{18}O$ record on speleothems at Minnetonka Cave (‰ VPDB, 42°N) in Idaho (Lundeen et al., 2013); and $\delta^{18}O$ record on endogenic carbonates (‰ VPDB) at Crevice Lake (45°N) in northern Yellowstone National Park (Whitlock et al., 2012). Net ice accretion (cm yr^{-1}) and $\delta^{18}O$ record data (‰ VSMOW) from the Beartooth ice patch core (Chellman et al., 2021). Air temperature anomalies generated from pollen data (MTWM: Mean Temperature of the Warmest Month) based on a suite of paleoclimatic data sets compiled from the mid-latitudes of North America from Shuman and Marsicek 2016.

4.1 Proxy Interpretation

4.1.1 Interpretation of BSi, TOC, and C/N Ratios

Yellowstone Lake has high concentrations of DSi in the water column throughout the year (~11.2 mg SiO_2 L^{-1}, Gemery-Hill et al., 2007). Therefore, diatom production is likely not limited by DSi. Additionally, BSi concentration is strongly influenced by changes in the abundance of different diatom species (Conley, 1988) relative to dilution by detrital input (represented by MS and Ti data, Fig. 3) and does not directly reflect overall diatom production. Increased production of large heavily-silicified diatom species, such as *Stephanodiscus yellowstonenesis* and *Aulacoseira subarctica*, is likely to have a bigger influence than equivalent production by less silicified species, including *Stephanodiscus minutulus*.

At the base of the core (1170–820 cm depth), BSi concentration varied greatly likely reflecting sedimentation regimes that alternated between high (low) detrital input (Ti, Fig. 3) and low (high) abundance of the heavily-silicified diatom species *Stephanodiscus yellowstonensis* and *Aulacoseira subarctica*. Relatively high BSi concentrations in the middle part of the core (820–350 cm depth) are explained as a result of high mineral detrital input and diatoms composed primarily by *S. minutulus*. The uppermost part of the core (50–0 cm depth, last 500 years) was depleted in BSi (Fig. 3), which we interpret as a function of a decrease in the heavily-silicified taxa, *A. subarctica* and *S. yellowstonensis*.

In sediments of deep, cold lakes, like Yellowstone Lake, diagenetic processes likely have a limited impact on sediment carbon and nitrogen composition (Eadie et al., 1990). Thus, the increase in TOC (1.5–3.3%) is largely a result of higher algal production. The increase in C/N ratios (6.8–10.9) up core reflects the added sediment contributions of terrestrial carbon, which has a high C/N ratio relative to the dominant algal input, with a low C/N ratio (Meyers et al., 2001).

4.1.2 Interpretation of Fossil Diatom Assemblages

Stephanodiscus minutulus is a high phosphorus specialist, with low nitrogen and DSi requirements (Lynn et al., 2003; Interlandi et al., 2003). In Yellowstone Lake, *S. minutulus* blooms earliest in spring during isothermal mixing (Interlandi et al., 1999; Theriot et al., 2006). *Aulacoseira subarctica* blooms in spring after *S. minutulus* but before the onset of stratification; it can persist in deep water (>20 m depth) into early summer (Interlandi et al., 1999). As a heavily-silicified species, *A. subarctica* also requires high DSi concentrations (Kilham et al., 1996). Large populations of *A. subarctica* indicate cool, early summers that prolong the duration of isothermal mixing and allow populations to grow and persist into summer. *Asterionella formosa* blooms in spring at approximately the same time as *A. subarctica* but slightly deeper in the water column. It requires high nitrogen and moderate-to-high DSi relative to phosphorus (Kilham et al., 1996; Michel et al., 2006; Berthon et al., 2014). Populations of *A. formosa* decrease at the onset of stratification. *A. formosa* is an opportunistic species that is one of the first to respond to nitrogen enrichment (Saros et al., 2005; Michel et al., 2006). Thus, factors that increase N and/or Si availability during spring months, including increased N in runoff, would favor increased *A. formosa* abundance. *Stephanodiscus yellowstonenesis*, endemic to Yellowstone Lake, is a summer species with the ability to grow at depth and in low light conditions (Kilham et al., 1996; Theriot et al., 2006). In historical records, *S. yellowstonenesis* was most abundant during intervals of drought and long, stable summer stratification (Kilham et al., 1996).

The trade-off between *Aulacoseria subarctica* and/or *Asterionella formosa* with *Stephanodiscus minutulus* populations is largely controlled by temperature and its influence on stratification. Thus, a shortened spring period of isothermal mixing created by either late ice-off and/or stronger summer stratification favors dominance by *S. minutulus* (Interlandi et al., 1999; Theriot et al., 2006), whereas below-average summer temperatures enable blooms of *A. subarctica* and *A. formosa* by delaying the onset of stratification or weakening stratification. As such, early or strong summer stratification truncates spring turnover before large populations of the late-spring species, *A. subarctica* and *A. formosa* become established.

4.1.3 Interpretation of $\delta^{18}O_{lake}$

$\delta^{18}O_{lake}$ (and δD_{lake}) are influenced by climate through changes in temperature, lake water balance, and precipitation sources (Leng and Barker, 2006). Because the diatom species selected for isotopic analysis, *Stephanodiscus yellowstonensis,* typically blooms in late June and develops large populations in summer (Theriot et al., 2006), the $\delta^{18}O_{diatom}$ record represents average $\delta^{18}O_{lake}$ after snowmelt and during the ice-free season. Each sediment sample (1 cm) in the YL16-2C core spans, on average, 8.4 years of sedimentation. Possible controls on $\delta^{18}O_{diatom}$ include water temperature at the time and place of diatom growth and $\delta^{18}O_{lake}$. $\delta^{18}O_{lake}$, in turn, is influenced by changes in temperature, evaporation, and lake-water balance and precipitation origin (Leng and Barker, 2006).

$\delta^{18}O_{diatom}$ values are affected by a temperature-dependent fractionation between water and diatoms, on average of -0.2 ‰/°C (Brandriss et al., 1998; Moschen et al., 2005). Variability in $\delta^{18}O_{diatom}$ (+2.9 ‰) implies unrealistic changes in lake-water temperature of 14–15 °C on average (Shuman and Marsicek, 2016). Therefore, water temperature likely accounts for only a small fraction of the observed variation in $\delta^{18}O_{diatom}$, and it is not the major factor influencing the record.

Lake water is well mixed, and evaporative forcing on $\delta^{18}O_{lake}$ was observed for samples collected in both 1998/1999 and 2018 (Fig. 6A; Balistrieri et al., 2007). The lake waters had higher $\delta^{18}O_{lake}$ in comparison to tributaries, precipitation, and snow. With a water residence time of 14±3 years (Balistrieri et al., 2007), the short-term impact of recharge after snowmelt, which lowers $\delta^{18}O_{lake}$, is limited to surface waters close to the major inflow. The YL16-2C coring site, which is ~3 km south of the outlet, reflects waters in the northern part of Yellowstone Lake, which are heavier as a result of surface evaporation as water flows 30 km through the lake from the Southeast Arm inlet (Fig. 6B).

The Yellowstone River delivers about 70% of annual water inflow (data from 1998 and 1999; Balistrieri et al., 2007), and interannual changes in its discharge (and more broadly that of all incoming streams) influence $\delta^{18}O_{lake}$. Because most precipitation at Yellowstone Lake occurs as snowfall, $\delta^{18}O_{lake}$ is expected to be affected by the amount of inflow and % snowmelt of that inflow. Modern winter and spring precipitation derives mainly from northern Pacific storm systems (Despain, 1987), whereas in summer, warmer subtropical moisture sources deliver precipitation with higher $\delta^{18}O$ (Anderson et al., 2016). Based on modern water isotopes from Yellowstone Lake and tributaries, evaporation drives a +3‰ shift from inlets to outflow, but snowfall has up to -6‰ shift from current inflow. Hereafter, changes in the $\delta^{18}O_{diatom}$ record are interpreted as changes in the contribution of lake-water evaporation relative to the contribution of stream inflow.

4.2 Climate Reconstruction from Yellowstone Lake Multiproxy Record

4.2.1 Early Holocene (9880 to 6700 cal yr BP)

High $\delta^{18}O_{diatom}$ values during this period (Fig. 7), particularly from 9880–7500 cal yr BP, are attributed to higher lake-water evaporation than present and/or reduced inflow linked to decreased winter/spring precipitation. In addition, increased water vapor from subtropical Pacific and Gulf of Mexico sources may have enriched ^{18}O content of precipitation from summer thunderstorms, as inferred in the Colorado Rockies (Anderson et al., 2016). A negative excursion in $\delta^{18}O_{diatom}$ is present at 7000–6800 cal yr BP, suggesting cooler and/or wetter conditions for a short period.

The abundance of *Pinus contorta*-type pollen in the early Holocene (Zone YL-P1) sediments at Yellowstone Lake falls within the range of modern pollen samples from *P. contorta* forests in the GYE (~55–95%, Iglesias et al., 2018). *Pinus albicaulis*-type pollen also was more abundant in the early Holocene (Zone YL-P1, Fig. 4), consistent with expansion of *P. albicaulis* or *P. flexilis* from 12,000-7000 cal yr BP in the GYE (Iglesias et al., 2015). Indicators of steppe vegetation, including *Artemisia*, Poaceae, and Amaranthaceae, were not abundant in the early Holocene. Theriot et al. (2006) suggest an expansion of riparian vegetation in Yellowstone Lake at 7000 cal yr BP based on high levels of *Salix* pollen in their core, but we did not observe a marked increase of riparian taxa in our record. Other records show that *P. contorta* was the dominant tree on various rhyolitic sites (Whitlock, 1993) and non-rhyolitic sites (Waddington and Wright, 1974; Baker, 1976) at this time, with only minor presence of other conifers. The Yellowstone Lake pollen record thus provides a good depiction of early-Holocene vegetation trends at a regional scale.

Large fire-episode frequency with small CHAR peak magnitudes suggest that fires were comparatively infrequent and small in the early Holocene (relative to Zone YL-P2). The dearth of fires may explain the low terrestrial organic matter input and decreased productivity at this time, as indicated by the low C/N and TOC ratios (Fig. 3).

Diatom assemblages dominated by *Stephanodiscus minutulus* (Fig. 5) indicate that lake waters were generally low in nitrogen, suggesting limited winter runoff, and high in phosphorus concentrations from spring isothermal mixing (Zone YL-D1). This period includes the first appearance of *S. yellowstonensis* in significant (>5%) abundance, suggesting years of sustained summer stratification (Kilham et al., 1996). The high abundance of *S. minutulus* combined with the appearance of substantive proportions of *S. yellowstonensis* suggest early snowmelt and ice-off in spring, with spring nutrient dynamics influenced by winter moisture followed by prolonged summer stratification (Fig. 5). The relatively high proportion of plankton relevant to tychoplankton and benthon taxa suggests minimal benthic habitat near the coring location, possibly as a result of higher lake levels (Fig. 7). This inference is consistent with exposed lake shorelines 5–6 m above present elevation that are dated to ~9000–7000 cal yr BP (S2 & S3 lake terraces of Pierce et al., 2007).

The inference of greater summer evaporation from the $\delta^{18}O$ record suggests that summer warmth and high evaporation rates had little influence on water depth at this time. In fact, the higher lake stands are attributed to cyclical deformation processes within the Yellowstone caldera, and caldera doming in the early Holocene explains the presence of exposed shorelines (Pierce et al., 2007). The relatively low BSi wt% and BSi fluxes in the early Holocene may be related to the overall dominance of the low-silica content species, *S. minutulus*, and relatively high detrital input (Ti) diluting the BSi concentration (Fig. 3).

In summary, the Yellowstone Lake data indicate that, during the early Holocene, $\delta^{18}O_{diatom}$-inferred summer evaporation was higher than present. *Pinus contorta* forests were more open or less extensive than present, possibly the result of high summer temperatures, greater aridity, and small fires. Summer stratification was prolonged following early snowmelt and ice-off. Dry conditions also resulted in comparatively low nutrient flux to the lake from the catchment. These observations are consistent with warmer springs and longer summer conditions than at present.

4.2.2 Middle Holocene (6700 to 3000 cal yr BP)

After high $\delta^{18}O_{diatom}$ values at ca. 6000 cal yr BP, values were low (Fig. 7) from 5800–4500 cal yr BP, suggesting reduced summer evaporation compared to the early Holocene, as well as a possible increase of snowmelt in tributary streams. Between 4500 and 3000 cal yr BP, $\delta^{18}O_{diatom}$ values departed from their middle Holocene trend (Fig. 7) and increase to values similar to those of the early Holocene. This shift suggests a higher summer evaporation and a reduced snowmelt influence on the $\delta^{18}O_{lake}$ signature. As in the early Holocene, a higher contribution of rain derived from subtropical vapor sources could also have accounted for the increase in $\delta^{18}O_{diatom}$ values. Within the middle Holocene, the interval 4500–3000 cal yr BP, is exceptional in showing paleohydrological conditions similar to those of the early Holocene.

Pinus pollen percentages increased in Zone YL-P2 (Fig. 4) and at other sites in the Yellowstone Lake vicinity, suggesting increased forest density or cover in the middle Holocene (Iglesias et al., 2018; Iglesias and Whitlock, 2020). Since the *Pinus* pollen is dominantly *P. contorta*-type, we infer closure or increased extent of *P. contorta* forest in the region (Fig. 7). The *Pinus* increase occurred at the expense of steppe taxa, chiefly *Artemisia*. Cygnet Lake (Whitlock, 1993) on the rhyolite plateau to the northwest of Yellowstone Lake recorded increased *Pinus* pollen percentages at this time, with negligible amounts of *Abies* and *Picea* pollen. Cub Creek Pond (Waddington and Wright, 1974) and Buckbean Fen (Baker, 1976), located on andesitic substrate in the eastern and southern part of the watershed, document increasing percentages of *Pinus*, *Abies*, and *Picea* indicating establishment of mixed conifer forests after ca. 5000 cal yr BP. The Yellowstone Lake record integrates the vegetation changes on both substrates within the watershed and, thus, shows increased percentages of all three conifer taxa.

The charcoal record suggests an increase in large fire episodes, reflecting greater area burned, higher fire severity, or closer fire proximity than before (Fig. 4). Today, closed *Pinus contorta* forests support infrequent, high-severity fires (Despain, 1990), and we assume that this vegetation and fire regime also characterized the middle Holocene, as well.

A marked increase in *Aulacoseira subarctica* after 6700 cal yr BP indicates longer periods of isothermal mixing (spring turnover) than in the early Holocene (Fig. 5). Intervals with increased *Asterionella formosa* (5500–5000 cal yrs BP, 4500–3000 cal yrs BP, 2000–1380 cal yrs BP) may have been a result of higher N input from increased runoff in spring, consistent with wetter winters (increased snowmelt) inferred from $\delta^{18}O_{diatom}$ values and charcoal evidence of infrequent fires (increased fuel build-up with in basin). Within the middle Holocene, the period from 5350–4900 cal yr BP is distinctive in the co-occurrence of high *A. subarctica*, *A. formosa*, and *Stephanodiscus yellowstonensis,* which suggests that this interval may have had extended summer stratification. Slight decreases in the P:T+B ratio between 4000 and 3000 cal yr BP indicate increasing benthic habitat during this period (Fig. 7), consistent with high $\delta^{18}O$ values and inferences of a low lake stand (Pierce et al., 2007).

The sediments between 825 and 350 cm depth (6800–2800 cal yr BP) are composed of diatom-rich laminae alternating with detrital-rich layers (Fig. 3). Higher BSi concentrations than before and higher total organic carbon content with C/N ratios of about 8 (indicative of algae) suggest increased in-lake biological production during this period (Fig. 3). Because the BSi flux shows stable accumulation rates with minor variations, which mimic the changes in MAR, the changes in BSi concentration likely represent the variation of in-lake BSi production. In general, variability in BSi concentration was driven by shifts in diatom species composition and detrital input, with positive excursions a result of higher abundance of the heavily-silicified species, *Stephanodiscus yellowstonensis* and *Aulacoseira subarctica*, and low detrital input.

To summarize, a combination of decreased evaporation and/or increased snowmelt inferred from $\delta^{18}O_{diatom}$ (7000–4500 cal yr BP), laminations of BSi-rich and mineral-rich sediments, diatom-inferred increases in nitrogen availability, and increased terrestrial organic material suggest wetter winters than during the early Holocene and, thus, a subsequent increase in runoff during a prolonged or delayed snowmelt and ice off followed by cool summers. During the middle Holocene, *P. contorta* forest in the watershed became denser, supplying fuel to propagate larger fire episodes than in the early Holocene.

4.2.3 Late Holocene (3000 to -67 cal yr BP)

$\delta^{18}O_{diatom}$ values decreased until 1200 cal yr BP, during a period of cooler conditions in the Rocky Mountain region, as evidenced by Neoglacial glacial advances (3000–1200 cal yr BP) (Menounos et al., 2009) and heavier $\delta^{18}O$ values obtained from an ice patch core in the Beartooth Mountains, northeast of Yellowstone National Park (Chellman et al., 2021). Values of $\delta^{18}O_{diatom}$ were slightly higher at ca. 2000 cal yr BP, during the Roman Warm Period (ca. 2200–1550 cal yr BP; Bianchi et al. 1999), suggesting warmer and/or drier conditions. This interval is registered as a period of dry summers and winters at Crevice Lake (Whitlock et al., 2012) (Fig. 8). Concurrent with climate change, rising lake levels from 3000 cal yr BP to present are inferred from submerged shorelines dating to 2900–2700 cal yr BP and suggest inflation of the Yellowstone caldera (Pierce et al., 2007).

A peak in $\delta^{18}O_{diatom}$ values occurred at ca. 1100 cal yr BP, during the Medieval Climate Anomaly (MCA) (1000–700 cal yr BP; Mann et al., 2009), indicating an increased evaporative component in the lake-water balance as a result of warmer and/or drier conditions than before; this was also observed at Bison Lake in Colorado (Fig. 8; Anderson, 2011). Finally, a shift to lower $\delta^{18}O_{diatom}$ values after ca. 1000 cal yr BP indicates less evaporation during the cooler and/or wetter conditions of the Little Ice Age (LIA 1550–1850 CE; Viau et al., 2012), consistent with isotope and diatom data from other lakes in the northern Rocky Mountains (Bracht and Fritz, 2012). At those sites, synchronous shifts in diatom assemblages suggest a regional transition to protracted cool springs and shorter summers with a moderate increase in effective moisture.

The late-Holocene pollen record from Yellowstone Lake shows little change from the middle Holocene. Cygnet Lake in the northwest featured the highest *Pinus* pollen percentages of that record, and other conifer pollen types remained nearly absent. In the eastern and southern part of the watershed, *Pinus* pollen percentages declined at Cub Creek Pond (Waddington and Wright, 1974) and remained steady at Buckbean Fen (Baker, 1976), as *Abies lasiocarpa* and *Picea engelmannii* became more abundant. Pollen percentages at Yellowstone Lake integrated the vegetation histories on the different substrates within the watershed and remained relatively constant in the late Holocene, reflecting the fact that *Pinus* became more abundant on rhyolitic substrates and less abundant on andesitic substrates.

The uppermost charcoal peaks are assigned to recent large fire events. Fire episodes ca. 1700 CE burned 100,000s of hectares in the Yellowstone Lake watershed (Romme and Despain, 1989; Tinker et al., 2003), and the 1988 CE fires, covered approximately 321,000 ha (Spatial Analysis Center, Yellowstone National Park, 2020). The charcoal record did not detect smaller historical fires that burned >4000 ha in the Yellowstone Lake watershed including the Flat Mountain (1910 CE), East (2003), Columbine (2007), and Arnica (2009) fires (Spatial Analysis

Center, Yellowstone National Park, 2020). Their absence supports the interpretation that charcoal peaks in large lakes register exceptionally large fire episodes, an observation that has been noted in other studies (Millspaugh and Whitlock, 1995; Thevenon and Anselmetti, 2007).

After 1500 cal yr BP, the diatom assemblage shifted towards a co-dominance of *Aulacoseira subarctica* and *Stephanodiscus minutulus* and higher overall *Asterionella formosa* abundance (Fig. 5). Increased relative abundance of *A. subarctica* and *A. formosa* in comparison with *S. minutulus* indicates extended periods of spring turnover (Fig. 7) in the late Holocene, which allowed large diatom blooms during late spring. Additionally, higher abundance of *A. formosa* implies high nitrogen input from the catchment (Wolfe et al., 2001), likely the result of wetter winters or springs than before (Kilham et al., 1996). *A. formosa* also increased at 1500-1200 cal yr BP at other sites in southwestern Montana (Bracht-Flyr and Fritz, 2012), suggesting a regional increase in winter/spring precipitation and spring runoff during the late Holocene. Decreased plankton: tychoplankton and benthon ratio indicates higher availability of benthic habitat closer to the coring location and, thus, lower lake level than the early or middle Holocene.

BSi fluxes steadily decreased, and TOC values slightly increased in the late Holocene, suggesting a slight increase in detrital input. High BSi concentrations parallel an increase in high-silica diatom species and, thus, reflect the increased production of *Aulacoseria subarctica* and *Stephanodiscus yellowstonensis*. Higher C/N ratios values in the late Holocene than before suggest a greater contribution of terrestrial organic matter in comparison to in-lake organic production (Fig. 3).

The generally lower BSi concentration in the upper part of the core may be a result of dilution of diatom silica from increased detrital minerals in runoff, as indicated by the Ti and

C/N records. Declines in BSi concentrations also were reported by Theriot et al. (2006) from 2200 cal yr BP to the present in Yellowstone Lake. Diatom assemblages from other northern Rocky Mountain lakes also suggest changes in seasonality towards longer, warm summers and decreased effective moisture 2200–2100 cal yrs BP (Bracht-Flyr and Fritz, 2012). These diatom changes may be a response to changes in nutrient patterns brought on by regional increases in precipitation.

Overall, the proxy data suggest continually decreasing summer evaporation and/or increasing snowmelt, and cool summers as summer insolation reached the lowest values of the Holocene (~468 W m^{-2}; Fig. 7; Laskar et al., 2004). The watershed supported a dense forest in the late Holocene, but of slightly different composition on rhyolite and non-rhyolite substrates, and large fires were evident. Diatom-inferred extended spring mixing suggests wetter winters and, thus, increased runoff during spring snowmelt. Low levels in BSi fluxes and TOC indicate higher detrital input.

4.3 Regional Comparisons within the GYE

4.3.1 Early Holocene

The early Holocene was characterized by warmer drier summers than present in central GYE, as a result of greater-than-present summer insolation and a strengthened northeastern Pacific subtropical high-pressure system (Bartlein et al., 1998; Renssen et al., 2012) (Fig. 7). Despite lower winter insolation at this time, model simulations suggest that the position and intensity of the winter westerly jet in the early Holocene changed little from the present (Zhou et al., 2020), implying that winter conditions in Yellowstone were colder but perhaps no wetter than present.

The $\delta^{18}O_{diatom}$ results are consistent with a $\delta^{18}O$ record of endogenic carbonates at Bison Lake, Colorado (a region highly influenced by the North American Monsoon), where positive anomalies were associated with a rain-dominated (relative to snow) precipitation regime (Fig. 8; Anderson, 2011). Net ice accretion in the Beartooth Mountains, Wyoming (Fig. 1) also slowed during the early Holocene, indicating less snowpack except between ca. 9000 and 7000 cal yr BP (Fig. 8, Chellman et al., 2021).

Paleoclimate reconstructions in the central Rocky Mountains generally indicate an early-Holocene period of higher air temperature and lower precipitation than the middle and late Holocene (Fig. 8; Shuman and Marsicek, 2016), consistent with the pattern inferred at Yellowstone Lake. In contrast, multiproxy records from northern Yellowstone show wetter summer conditions at Crevice Lake and Slough Creek Pond (Whitlock et al., 2012), both in the summer-wet region. Wetter conditions also are recorded southwest of Yellowstone National Park, based on the $\delta^{18}O$ record of Minnetonka Cave in Idaho (Fig. 8; Lundeen et al., 2013).

4.3.2 Middle Holocene

The general trend of increasing precipitation and decreased temperatures is evident in the regional paleoclimate synthesis of Shuman and Marsicek (2016) and the $\delta^{18}O$ record of Bison Lake, Colorado (Anderson, 2011). In contrast, the $\delta^{18}O$ data at Crevice Lake in northern Yellowstone indicates a trend towards drier winters (Whitlock et al., 2012; Fig. 8). The $\delta^{18}O$ record from the Beartooth ice patch suggests increasing winter temperatures, and a composite air temperature reconstruction from pollen data from the mid-latitudes in North America shows cooling during the warmest month of the year (Shuman and Marsicek, 2016; Fig. 8). Together, these records indicate a trend towards cooler, wetter conditions during the middle Holocene.

A climate excursion is noted in several of the records between ca. 4500 and 3000 cal yr BP. The Beartooth ice patch $\delta^{18}O$ record indicates relatively warm temperatures at ca. 4100 cal yr BP (Fig. 8; Chellman et al., 2021). In contrast, Crevice Lake (Whitlock et al., 2012) records an interval of anoxic bottom-waters between 4400 and 3900 cal yr BP, suggesting a period of deep lake and wetter conditions in northern GYE (Fig. 8). The Beartooth ice patch $\delta^{18}O$ data and regional temperature composite record suggest that this excursion ended between 3900–3000 cal yr BP and was followed by a return to cooler conditions in winter and during the warmest month of the year (Fig. 8).

4.3.3 Late Holocene

Other regional paleoclimate records suggest cooler and wetter conditions during the late Holocene, similar to the climate recorded in Yellowstone Lake. The $\delta^{18}O$ records of Minnetonka Cave, southwest of Yellowstone and Bison Lake, south of Yellowstone support this interpretation (Fig. 8). In addition, the stack of regional lake-level reconstructions and of temperature during warmest month indicate increasing lake levels and lower temperatures than during Early Holocene (Fig. 8; Shuman and Marsicek, 2016). Winter and summer temperatures were low in Wyoming according to the record of Beartooth ice patch $\delta^{18}O$ data and the summer insolation anomalies (Fig. 8). Recent centuries are characterised by a trend towards slightly higher summer temperatures than much of last three millennia. In addition to increases in $\delta^{18}O_{diatom}$ values at Yellowstone Lake, $\delta^{18}O$ increases are noted at Minnetonka Cave and Bison Lake (Fig. 8).

5. Conclusions

Paleoenvironmental proxies from an 1182-cm-long composite sediment core trace the watershed and limnological history of Yellowstone Lake from 9880 to -67 cal yr BP. Most changes in terrestrial and limnological ecosystems were gradual and attributed to slowly varying changes in the seasonal cycle of insolation within the GYE, which led to warm, dry summer conditions in the early Holocene and progressively cooler wetter conditions in middle and late Holocene. However, the record also highlighted periods of more abrupt environmental changes, which can be attributed to climate events previously poorly documented in the region. In particular, succession of submillenial climate oscillations occurred during the middle Holocene (7000–6800 cal yr BP). Distinct warming also registered from 4500–3000 cal yr BP and during the MCA.

The early Holocene (9880–6300 cal yr BP) climate supported an open or less dense forest in the watershed, small frequent fires, high lake-water evaporation rates in summer and/or reduced snowpack in winter and early spring snowmelt, generally low nutrient availability, and early ice-off followed by extended lake stratification. Middle Holocene (6300–3000 cal yr BP) cooling led to the establishment of a denser pine forest and larger fire episodes than before, as well as less summer evaporation and/or increased stream input of winter or spring precipitation. Increased or longer spring runoff during the middle Holocene is inferred from increased abundance of diatom species that require high nitrogen concentrations. Further cooling and increased moisture in the late Holocene (3000–-67 cal yr BP) resulted in the development of closed forest, infrequent large fire episodes, and high inputs of terrestrial organic matter to the lake. Decreasing summer evaporation and/or increased snowmelt relative to the mid-Holocene also is consistent with cooler conditions.

Although previous investigations have examined various aspects of climate history of the Yellowstone region with different sets of proxy records, our study offers the first high-resolution hydroclimatic record for the region based on $\delta^{18}O_{diatom}$ data and also an examination of how past climate variations influenced terrestrial and limnic responses in a large watershed in the central part of the Yellowstone region. The proxies clearly show that the Yellowstone Lake watershed had a climate history typical of a summer-dry region, in which conditions were warmest and driest in the early Holocene as a result of the summer insolation maximum and the expansion of the northeastern Pacific subtropical high-pressure system. The climate become cooler and wetter in the middle and late Holocene reaching the pre-industrial “present”. Superimposed on these slowly varying trends, the climate record shows submillennial excursions that are best reflected in the limnobiotic and fire data. Additionally, our proxy record indicated minimal influence of climate on lake level, indicating caldera deformation may have a stronger influence than climate on water depth and shoreline development.

In contrast, the vegetation history is clearly a regional reconstruction, integrating the changes in plant communities on different substrates within the watershed. These different responses of terrestrial and limnological components of the Yellowstone Lake watershed to past climate change points to the value of multi-proxy studies at a single site, as an opportunity to improve paleoenvironmental interpretations. This suite of paleoenvironmental proxies from Yellowstone Lake provides marked evidence that the sensitive ecosystems of Yellowstone National Park have been substantially influenced by climate influences on multiple scales.

Acknowledgements

This research was supported by the National Science Foundation's Integrated Earth Systems program EAR-1516361 (Morgan, Shanks), EAR-1515353 (Whitlock), and EAR-1515377 (Fritz), the Swedish Research Council (Conley), The Royal Physiographic Society in Lund (to both Cartier and Zahajská), and a Swedish Research Council Tage Erlander Professorship (Fritz). The research was conducted under Yellowstone National Park research permits YELL-2016-SCI-7018, YELL-2016-SCI-5054, YELL-2018-SCI-5054 and YELL-2018-SCI-7084. Yellowstone Lake coring was aided by M. Baker, C. Linder, R. O'Grady, M. Shapley, R. Sohn, and Yellowstone National Park rangers. LacCore provided coring infrastructure, laboratory space for core splitting, subsampling, and analyzes including magnetic susceptibility. We thank K. Ljung for his help in the analysis of organic matter and C. Alwmark for assistance with the SEM at Lund University. Any use of trade, firm, or product names is for descriptive purposes only and does not imply endorsement by the U.S. Government.

Declaration of competing interests

The authors have no competing interests to declare.

References

Anderson, L., 2011. Holocene record of precipitation seasonality from lake calcite $\delta^{18}O$ in the central Rocky Mountains, United States. Geology 39, 211–214. https://doi.org/10.1130/G31575.1

Anderson, L., Berkelhammer, M., Barron, J.A., Steinman, B.A., Finney, B.P., Abbot, M.B., 2016. Lake oxygen isotopes as recorders of North American Rocky Mountain hydroclimate: Holocene patterns and variability at multi-decadal to millennial time scales. Glob. Planet.

Change 137, 131–148. https://doi.org/10.1016/j.gloplacha.2015.12.021

Anderson, J.E., Romme, W.H., 1991. Initial floristics in lodgepole pine (*Pinus contorta*) forests following the 1988 Yellowstone fires. Int. J. Wildland Fire 1(2), 119–124. doi:10.1071/WF9910119

Bahls, L., 2005. Northwest diatoms: a photographic catalogue of species in the Montana Diatom Collection, with ecological optima, associates, and distribution records for the nine northwestern United States. In: Northwest diatoms, Volume 2. The Montana Diatom Collection, Helena, 464 pp.

Baker, R.G., 1976. Late Quaternary vegetation history of the Yellowstone Lake basin, Wyoming. U.S.Geological Survey Professional Paper 729E, pp. 1–48. https://doi.org/10.3133/pp729E

Balistrieri, L., Shanks, W.C.P., Cuhel, R.L., Augilar, C., Klump, J.V., 2007. The influence of sub-lacustrine hydrothermal vents on the geochemistry of Yellowstone Lake. Chapter F of: Morgan, L.A. (ed.), Integrated Geoscience Studies in the Greater Yellowstone Area--Volcanic, Tectonic, and Hydrothermal Processes in the Yellowstone Geoecosystem, U.S. Geological Survey Professional Paper 1717, p. 169–200. https://doi.org/10.3133/pp1717.

Bartlein, P.J., Anderson, K.H., Anderson, P.M., Edwards, M.E., Mock, C.J., Thompson, R.S., Webb, R.S., Webb, T., Whitlock, C., 1998. Paleoclimate simulations for North America over the past 21,000 years: Features of the simulated climate and comparisons with paleoenvironmental data. Quat. Sci. Rev. 17, 549–585. https://doi.org/10.1016/S0277-3791(98)00012-2

Battarbee, R.W., 2003. Diatom Analysis. In: Berglund, B., Ralska-Jasiewicowa, M. (eds.), Handbook of Holocene Palaeoecology and Palaeohyrology. Blackburn Press, Caldwell, NJ, pp. 527–570.

Bennett, K., Willis, K., 2001. Pollen. In: Mol, J., Birks, H.J.B., Last, W.M. (eds.), Tracking Environmental Change Using Lake Sediments. Volume 3: Terrestrial, Algal, and Siliceous Indicators. Kluwer Academic Publishers, Dordrect, pp. 5–32.

Berthon, V., Alric, B., Rimet, F., Perga, M., 2014. Sensitivity and responses of diatoms to climate warming in lakes heavily influenced by humans. Freshw. Biol. 59, 1755–1767. https://doi.org/10.1111/fwb.12380

Bianchi, G.G., McCave, I.N., 1999. Holocene periodicity in North Atlantic climate and deep-ocean flow south of Iceland. Nature 397(6719), 515–7. doi:10.1038/17362

Blaauw, M., Christen, J.A., 2011. Flexible paleoclimate age-depth models using an autoregressive gamma process. Bayesian Anal. 6, 457–474. https://doi.org/10.1214/11-BA618

Bouligand, C., Tivey, M.A., Finn, C.A., Morgan, L.A., Shanks, W.C.P., Sohn, R.A., 2020. Geological and thermal control of the hydrothermal system in northern Yellowstone Lake: Inferences from high-resolution magnetic surveys. J. Geophys. Res. Solid Earth 125, e2020JB019743. https://doi/org/10.1029/2020JB019743

Boyd, C.E. (ed.), 2012. Bottom soils, sediment, and pond aquaculture. Springer Science & Business Media, 348 p. https://doi.org/10.1007/978-1-4615-1785-6

Bracht-Flyr, B., Fritz, S.C., 2012. Synchronous climatic change inferred from diatom records in four western Montana lakes in the U.S. Rocky Mountains. Quat. Res. 77, 456–467. https://doi.org/10.1016/j.yqres.2011.12.005

Brandriss, M.E., O’Neil, J.R., Edlund, M.B., Stoermer, E.F., 1998. Oxygen isotope fractionation between diatomaceous silica and water. Geochim. Cosmochim. Acta 62, 1119–1125. https://doi.org/10.1016/S0016-7037(98)00054-4

Cash, R., 2015. Multibeam echosounding as a tool for mapping geologic features, bathymetry and modern vents, Yellowstone National Park, Wyoming. Master of Science thesis., University of Illinois Champain-Urbana, 133 p.

Chellman, N.J., Pederson, G.T., Lee, C.M., McWethy, D.B., Puseman, K., Stone, J.R., Brown, S.R., McConnell, J.R., 2021. High elevation ice patch documents Holocene climate variability in the northern Rocky Mountains. Quat. Sci. Adv. 3, 100021. https://doi.org/10.1016/j.qsa.2020.100021

Christiansen, R.L., 2001. The Quaternary and Pliocene Yellowstone Plateau volcanic field of Wyoming, Idaho, and Montana: U.S. Geological Survey Professional Paper 729-G, 145 p., 3 Plates. https://doi.org/10.3133/pp729G

Clayton, R.N., Mayeda, T.K., 1963. The use of bromine pentafluoride in the extraction of oxygen from oxides and silicates for isotopic analysis. Geochim. Cosmochim. Acta 27, 43–52. https://doi.org/10.1016/0016-7037(63)90071-1

Conley, D.J., 1988. Biogenic silica as an estimate of siliceous microfossil abundance in Great Lakes sediments. Biogeochemistry 6, 161–179. https://doi.org/10.1007/BF02182994

Conley, D.J., Schelske, C.L., 2001. Biogenic Silica. In: Smol, J.P., Birks, H.J.B., Last, W.M. (eds.), 2001. Tracking Environmental Change Using Lake Sediments. Volume 3: Terrestrial, Algal, and Siliceous Indicators. Kluwer Academic Publishers, Dordrecht, The Netherlands. pp. 371. ISBN 978-0-306-47668-6

DeMaster, D.J., 2003. The diagenesis of biogenic silica: chemical transformations occurring in the water column, seabed, and crust, Treatise on Geochem. 7, 407. DOI: 10.1016/B0-08-043751-6/07095-X

Despain, D.G., 1990. Yellowstone vegetation: consequences of environment and history in a natural setting. Roberts Rinehart Publishers, Boulder, CO. ISBN: 978-0911797756

Despain, D.G., 1987. The two climates of Yellowstone National Park. Proc. Mont. Acad. Sci. 47, 11–20.

Dirks, R.A., Martner, B.E., 1982. The climate of Yellowstone and Grand Teton National Parks. U.S. Dep. Inter. Natl. Park Serv. Occas. Pap. No. 6. https://irma.nps.gov/DataStore/DownloadFile/550753

Eadie, B.J., Morehead, N.R., Landrum, P.F., 1990. Three-phase partitioning of hydrophobic organic compounds in Great Lake waters. Chemosphere 20, 161–178. https://doi.org/10.1016/0045-6535(90)90094-A

Egan, J., Staff, R., Blackford, J., 2015. A high-precision age estimate of the Holocene Plinian eruption of Mount Mazama, Oregon, USA. Holocene 25, 1054–1067. https://doi.org/10.1177/0959683615576230

Fritz, S.C., Anderson, N.J., 2013. The relative influences of climate and catchment processes on Holocene lake development in glaciated regions. J Paleolimnology 49, 349–362. https://doi.org/10.1007/s10933-013-9684-z

Gemery-Hill, P.A., Shanks, W.C.P., Balistrieri, L.A., Lee, G.K., 2007. Geochemical data for selected rivers, lake waters, hydrothermal vents, and subaerial geysers in Yellowstone National Park, Wyoming and vicinity, integrated geoscience studies of the Greater Yellowstone Area - volcanic, tectonic, and hydrothermal, Chapter L of Morgan, L.A. (ed.), Integrated Geoscience Studies in the Greater Yellowstone Area--Volcanic, Tectonic, and Hydrothermal Processes in the Yellowstone Geoecosystem. U.S. Geological Survey Professional Paper 1717, pp. 365–426. https://doi.org/10.3133/pp1717.

Higuera, P.E., Brubaker, L.B., Anderson, P.M., Hu, F.S, Brown, T.A., 2009. Vegetation mediated the impacts of postglacial climate change on fire regimes in the south-central Brooks Range, Alaska. Ecol. Monogr. 79(2), 201–219. https://doi.org/10.1890/07-2019.1

Higuera, P.E., Whitlock, C., Gage, J.A., 2011. Linking tree-ring and sediment-charcoal records to reconstruct fire occurrence and area burned in subalpine forests of Yellowstone National Park, USA. Holocene. 21(2), 327–341. https://doi.org/10.1177%2F0959683610374882

Hostetler, S., Whitlock, C., Shuman, B., Liefert, D., Drimal, C., Bischke, S. 2021. Greater Yellowstone Climate Assessment: past, present, and future climate change in Greater Yellowstone watersheds. Bozeman MT: Montana State University, Institute on Ecosystems. https://doi.org/10.15788/GYCA2021

Huerta, M.A., Whitlock, C., Yale, J., 2009. Holocene vegetation-fire-climate linkages in northern Yellowstone National Park, USA. Palaeogeogr. Palaeoclimatol. Palaeoecol. 271, 170–181. https://doi.org/10.1016/j.palaeo.2008.10.015

Iglesias, V., Krause, T.R., Whitlock, C., 2015. Complex response of white pines to past environmental variability increases understanding of future vulnerability. PLoS One 10, 1–12. https://doi.org/10.1371/journal.pone.0124439

Iglesias, V., Whitlock, C., 2020. If the trees burn, is the forest lost? Past dynamics in temperate forests help inform management strategies. Phil. Trans. R. Soc. B. 375, 20190115. https://doi.org/doi:10.1098/rstb.2019.0115

Iglesias, V., Whitlock, C., Krause, T.R., Baker, R.G., 2018. Past vegetation dynamics in the Yellowstone region highlight the vulnerability of mountain systems to climate change. J. Biogeogr. 45, 1768–1780. https://doi.org/10.1111/jbi.13364

Interlandi, S., Kilham, S., Theriot, E., 1999. Responses of phytoplankton to varied resource availability in large lakes of the Greater Yellowstone Ecosystem. Limnol. Oceanogr. 44(2),

668–682. http://dx.doi.org/10.4319/lo.1999.44.3.0668
Interlandi, S.J., Kilham, S.S., Theriot, E.C., 2003. Diatom-chemistry relationships in Yellowstone Lake (Wyoming) sediments: Implications for climatic and aquatic processes research. Limnol. Oceanogr. 48(1), 79–92. https://doi.org/10.4319/lo.2003.48.1.0079
Jacobson, G.L., Bradshaw, R.H.W., 1981. The selection of sites for paleovegetational studies. Quat. Res. 16, 80–96. https://doi.org/10.1016/0033-5894(81)90129-0
Johnson, S.Y., Stephenson, W.J., Morgan, L.A., Shanks, W.C.P., Pierce, K.L., 2003. Hydrothermal and tectonic activity in northern Yellowstone Lake, Wyoming. Bull. Geol. Soc. Am. 115, 954–971. https://doi.org/10.1130/B25111.1
Juggins, S., 2017. rioja: analysis of Quaternary science data, R package version (21). http://cran.r-project.org/package=rioja.
Keiter, R.B., Boyce, M.S., 1994. The Greater Yellowstone ecosystem: redefining America's wilderness heritage. Yale University Press, 428 p. ISBN: 0300059272, 9780300059274
Kelts, K., Briegel, U., Ghilardi, K., Hsu, K., 1986. The limnogeology-ETH coring system. Swiss J. Hydrol. 48, 104–115. https://doi.org/10.1007/BF02544119
Kilham, S.S., Theriot, E.C., Fritz, S.C., 1996. Linking planktonic diatoms and climate change in the large lakes of the Yellowstone ecosystem using resource theory. Limnol. Oceanogr. 41, 1052–1062. https://doi.org/10.4319/lo.1996.41.5.1052
Laskar, J., Robutel, P., Joutel, F., Gastineau, M., Correia, A.C.M., Levrard, B., 2004. A long-term numerical solution for the insolation quantities of the Earth. Astron. Astrophys. 428, 261–285. https://doi.org/10.1051/0004-6361:20041335
Leng, M.J., Barker, P.A., 2006. A review of the oxygen isotope composition of lacustrine diatom silica for palaeoclimate reconstruction. Earth-Science Rev. 75, 5–27.

https://doi.org/10.1016/j.earscirev.2005.10.001

Leng, M.J., Sloane, H.J., 2008. Combined oxygen and silicon isotope analysis of biogenic silica. J. Quat. Sci. Publ. Quat. Res. Assoc. 23, 313–319. https://doi.org/10.1002/jqs.1177

Licciardi, J.M., Pierce, K.L., 2018. History and dynamics of the Greater Yellowstone glacial system during the last two glaciations. Quat. Sci. Rev. 200, 1–33. https://doi.org/https://doi.org/10.1016/j.quascirev.2018.08.027

Locke, W.W., Meyer, G.A., 1994. A 12,000-year record of vertical deformation across the Yellowstone caldera: The shorelines of Yellowstone Lake. J. Geophys. Res. Solid Earth, 99 (B10), p. 20,079-20,094. https://doi.org/10.1029/94JB00243

Lundeen, Z., Brunelle, A., Burns, S., Polyak, V., Asmerom, Y., 2013. A speleothem record of Holocene paleoclimate from the northern Wasatch Mountains, southeast Idaho, USA. Quat. Int. 310, 83–95. https://doi.org/10.1016/j.quaint.2013.03.018

Lynn, S.G, Kilham, S.S., Kreeger, D.A., Interlandi, S.J., 2003. Effect of nutrient availability on the biochemical and elemental stoichiometry in the freshwater diatom *Stephanodiscus minutulus* (bacillariophyceae). J. Phycol. 36(3), 510–522. https://doi.org/10.1046/j.1529-8817.2000.98251.x

Mann, M.E., Zhang, Z., Rutherford, S., Bradley, R.S., Hughes, M.K., Shindell, D., Ammann, C., Faluvegi, G., Ni, F., 2009. Global signatures and dynamical origins of the Little Ice Age and Medieval Climate Anomaly. Science 326(5957), 1256–1260. https://doi.org/10.1126/science.1177303

Menounos, B., Osborn, G., Clague, J.J., Luckman, B.H., 2009. Latest Pleistocene and Holocene glacier fluctuations in western Canada. Quat. Sci. Rev. 28, 2049–2074. https://doi.org/10.1016/j.quascirev.2008.10.018

Meyer, G.A., Locke, W.W., 1986. Origin and deformation of Holocene shoreline terraces, Yellowstone Lake, Wyoming. Geology 14, 699-702. https://doi.org/10.1130/0091-7613(1986)14<699:oadohs>2.0.co;2o

Meyers, P.A., Teranes, J.L., Last, W.M., Smol, J.P., 2001. Sediment Organic Matter. In: Tracking Environmental Change Using Lake Sediments: Volume 2: Physical and Geochemical Methods. pp. 293–271. https://doi.org/10.1007/0-306-47670-3

Michel, T.J., Saros, J.E., Interlandi, S.J., Wolfe, A.P., 2006. Resource requirements of four freshwater diatom taxa determines by *in situ* growth bioassays using natural populations of alpine lakes. Hydrobiologia 568, 235-243. https://doi.org/10.1007/s10750-006-0109-0

Millspaugh, S.H., Whitlock, C., 1995. A 750-year fire history based on lake sediment records in central Yellowstone National Park, USA. Holocene 5(3), 283–292. https://doi.org/ 10.1177/095968369500500303

Millspaugh, S.H., Whitlock, C., Bartlein, P.J., 2000. Variations in fire frequency and climate over the past 17,000 yr in central Yellowstone National Park. Geology 28, 211–214. https://doi.org/10.1130/0091-7613(2000)28<211:VIFFAC>2.0.CO;2

Morgan, L.A., Shanks, W.C. P., Lee, G.K., Webring, M.W., 2007a. Bathymetry and Geology of the floor of Yellowstone Lake, Yellowstone National Park, Wyoming, Idaho, and Montana. U.S. Geological Survey Scientific Investigations Map 2973, 2 plates. https://doi.org/10.3133/sim2973.

Morgan, L.A., Shanks, W.C.P, Pierce, K.L., Lovalvo, D.A., Lee, G.K., Webring, M.W., Stephenson, W.J., Johnson, S.Y., Harlan, S.S., Schulze, B., Finn, C., 2007b. The floor of Yellowstone Lake is anything but quiet- new discoveries from high-resolution sonar imaging, seismic-reflections profiling, and submersible studies, Chapter D of Morgan, L.A.

(ed.), Integrated Geoscience Studies in the Greater Yellowstone Area--Volcanic, Tectonic, and Hydrothermal Processes in the Yellowstone Geoecosystem. U.S. Geological Survey Professional Paper 1717. p. 91–126, https://doi.org/10.3133/pp1717.

Morgan, L., Shanks W.C.P., Lovalvo, D., Johnson, S., Stephenson, W., Pierce, K., Harlan, S., Finn, C., Lee, G., Webring, M., Schulze, B., Dühn, J., Sweeney, R., Balistrieri, L., 2003. Exploration and discovery in Yellowstone Lake: results from high-resolution sonar imaging, seismic reflection profiling, and submersible studies. J. Volcanol. Geotherm. Res. 122, 221–242. https://doi.org/10.1016/S0377-0273(02)00503-6

Morgan, L.A., Shanks, W.C.P. Pierce, K., Iverson, N., Schiller, C., Brown, S.R., Zahajska, P., Cartier, R., Cah, R., Best, J., Whitlock, C., Fritz, S., Lowers, H., Benzel, W., Lovalvo, D., 2021. The dynamic floor of Yellowstone Lake: The last 14-ky of hydrothermal explosions, doming, faulting, and slumping. Submitted to Bull. Geol. Soc Am , MS#: B36190.

Morgan, L.A., Shanks, W.C.P., Pierce, K.L., 2009. Hydrothermal processes above the Yellowstone magma chamber: large hydrothermal systems and large hydrothermal explosions. Geol. Soc. Am. Spec. Pap. 459, 98. https://doi.org/10.1130/SPE459

Morgan, P., Blackwell, D.D., Spafford, R.E., Smith, R.B., 1977. Heat flow measurements in Yellowstone Lake and thermal structure of the Yellowstone Caldera. J. Geophys. Res. Solid Earth 82, 3719–3732. https://doi.org/10.1029/JB082i026p03719

Morley, D.W., Leng, M.J., Mackay, A.W., Sloane, H.J., Rioual, P., Battarbee, R.W., 2004. Cleaning of lake sediment samples for diatom oxygen isotope analysis. J. Paleolim. 31, 391–401. https://doi.org/10.1023/B:JOPL.0000021854.70714.6b

Morrison, J., Brockwell, T., Merren, T., Fourel, F., Phillips, A.M., 2001. On-line high-precision stable hydrogen isotopic analyzes on nanoliter water samples. Anal. Chem. 73, 3570–3575.

https://doi.org/10.1021/ac001447t

Moschen, R., Lücke, A., Schleser, G.H., 2005. Sensitivity of biogenic silica oxygen isotopes to changes in surface water temperature and palaeoclimatology. Geophys. Res. Lett. 32, 1–4. https://doi.org/10.1029/2004GL022167

NOAA dataset, 1988-2018. National Oceanic and Atmospheric Administration. National centers for environmental information. Climate data online: dataset discovery. Station: Lake Yellowstone, WY US USC00485345. Available online: https://www.ncdc.noaa.gov/cdo-web/datasets.

Pierce, K.L., Cannon, K.L., Meyer, G.A., Trebesch, M.J., Watts, R.D., 2007. Post-glacial inflation-deflation cycles, tilting, and faulting in the Yellowstone Caldera based on Yellowstone Lake shorelines, Chapter E of Morgan, L.A. (ed.), Integrated Geoscience Studies in the Greater Yellowstone Area--Volcanic, Tectonic, and Hydrothermal Processes in the Yellowstone Geoecosystem: U.S. Geological Survey Professional Paper 1717, pp. 127–168. https://doi.org/10.3133/pp1717.

Ragueneau, O., Gallinari, M., Corrin, L., Grandel, S., Hall, P., Hauvespre, A., Lampitt, R.S., Rickert, D., Stahl, H., Tengberg, A., Witbaard, R., 2001. The benthic silica cycle in the Northeast Atlantic: annual mass balance, seasonality, and importance of non-steady-state processes for the early diagenesis of biogenic opal in deep-sea sediments. Prog. Oceanogr. 50, 171–200. https://doi.org/https://doi.org/10.1016/S0079-6611(01)00053-2

Reimer, P.J., Bard, E., Bayliss, A., Beck, J.W., Blackwell, P.G., Ramsey, C.B., Buck, C.E., Cheng, H., Edwards, R.L., Friedrich, M., Grootes, P.M., Guilderson, T.P., Haflidason, H., Hajdas, I., Kaiser, K.F., Kromer, B., Manning, S.W., Niu, M., Reimer, R.W., Richards, D.A., Scott, E.M., Southon, J.R., Staff, R.A., Turney, C.S.M., van der Plicht, J., 2013.

IntCal13 and Marine13 Radiocarbon Age Calibration Curves 0–50,000 Years cal BP. Radiocarbon 55, 1869–1887. https://doi.org/10.2458/azu_js_rc.55.16947

Renssen, H., Seppä, H., Crosta, X., Goosse, H., Roche, D.M., 2012. Global characterization of the Holocene Thermal Maximum. Quat. Sci. Rev. 48, 7–19. https://doi.org/10.1016/j.quascirev.2012.05.022

Richmond, G.M., 1977. Surficial geologic history of the Canyon Village Quadrangle, Yellowstone National Park, Wyoming, for use with Map I-652. U.S.Geological Survey Bulletin 1427. https://doi.org/10.3133/b1427

Romme, W.H., Despain, D.G., 1989. Historical perspective on the Yellowstone fires of 1988. Biosci. 39, 695–699. https://doi.org/10.2307/1311000

Saros, J.E., Michel, T.J., Interlandi, S.J., Wolfe, A.P., 2005. Resource requirements of *Asterionella formosa* and *Fragilaria crotonensis* in oligotrophic alpine lakes: implications for recent phytoplankton community reorganizations. Can. J. Fish. Aquat. Sci. 62, 1681–1689. https://doi.org/10.1139/f05-077

Schiller, C.M., Whitlock, C., Alt, M., Morgan, L.A., 2020. Vegetation responses to Quaternary volcanic and hydrothermal disturbances in the Northern Rocky Mountains and Greater Yellowstone Ecosystem (USA). Palaeogeogr. Palaeoclimatol. Palaeoecol. 559, 109859. https://doi.org/10.1016/j.palaeo.2020.109859

Schiller, C.M., Whitlock, C., Elder, K.L., Iverson, N.A., Abbott, M.B., 2021. Erroneously old radiocarbon ages from terrestrial pollen concentrates in Yellowstone Lake, Wyoming, USA. Radiocarbon 63, 1–22. doi:10.1017/RDC.2020.118

Schoennagel, T., Turner, M.G., Romme, W.H., 2003. Influence of fire interval and serotiny on postfire lodgepole pine density in Yellowstone National Park. Ecology 84, 2967–2978. https://doi.org/10.1007/s10980-006-0028-5

Shanks, W.C.P., Morgan, L.A., Benzel, W.M., Mills, C.T., Moscati, R.J., 2019. Geochemistry of Hydrothermally Altered Sediments, Pore Fluids, and Hydrothermal Explosion Deposits from Yellowstone Lake. AGU Annual Meeting Abstract, abstract # V33D-0207

Shanks, W.C.P., Alt, J.C., Morgan, L.A., 2007. Geochemistry of sub-lacustrine hydrothermal deposits in Yellowstone Lake: hydrothermal reactions, stable isotope systematics, sinter deposition, and spire growth, integrated geoscience studies of the Greater Yellowstone Area - volcanic, tectonic, and hydrothermal, Chapter G of Morgan, L.A. (ed.), Integrated Geoscience Studies in the Greater Yellowstone Area--Volcanic, Tectonic, and Hydrothermal Processes in the Yellowstone Geoecosystem. U.S. Geological Survey Professional Paper 1717, pp. 201–234. https://doi.org/10.3133/pp1717.

Shuman, B.N., Marsicek, J., 2016. The structure of Holocene climate change in mid-latitude North America. Quat. Sci. Rev. 141, 38–51. https://doi.org/10.1016/j.quascirev.2016.03.009

Smith, R.B., Jordan, M., Steinberger, B., Puskas, C.M., Farrell, J., Waite, G.P., Husen, S., Chang, W.L., O'Connell, R., 2009. Geodynamics of the Yellowstone hotspot and mantle plume: Seismic and GPS imaging, kinematics, and mantle flow: J. Volcan. Geotherm. Res. 188, 26–56. https://doi.org/10.1016/j.jvolgeores.2009.08.020

Spatial Analysis Center, Yellowstone National Park, 2020. Fire Perimeters (from 1881 to 2018) in Yellowstone National Park, Wyoming, Montana, Idaho: Spatial Analysis Center, Yellowstone National Park. https://irma.nps.gov/DataStore/Reference/Profile/2188228#.

Spaulding, S., Edlund, M., 2019. Diatoms of North America. Retrieved March 25, 2019, from https://diatoms.org/genera

Strickland, J., and Parsons, T., 1972. A Practical Handbook of Seawater Analysis, Second Edition, Fisheries Research Board of Canada, Bulletin no. 167. ISBN: B0007AFUR6

Sugita, S., 1993. A model of pollen source area for an entire lake surface. Quat. Res. 39, 239–244. https://doi.org/10.1006/qres.1993.1027

Swann, G.E., Leng, M.J., Sloane, H.J., Maslin, M.A., Onodera, J., 2007. Diatom oxygen isotopes: evidence of a species effect in the sediment record. Geochem. Geophys. Geosyst. 8, 1–10. https://doi.org/10.1029/2006GC001535

Theriot, E.C, Fritz, S.C., Gresswell, R.E., 1997. Long-term limnological data from the larger lakes of Yellowstone National Park, Wyoming, U.S.A. Arct. Alp. Res. 29(3), 304–314. https://doi.org/10.2307/1552145

Theriot, E.C., Fritz, S.C., Whitlock, C., Conley, D.J., 2006. Late Quaternary rapid morphological evolution of an endemic diatom in Yellowstone Lake, Wyoming. Paleobio. 32, 38–54. https://doi.org/10.1666/02075.1

Thevenon, F., Anselmetti, F.S., 2007. Charcoal and fly-ash particles from Lake Lucerne sediments (Central Switzerland) characterized by image analysis: anthropologic, stratigraphic and environmental implications. Quat. Sci. Rev. 26(19–21), 2631–2643. https://doi.org/10.1016/j.quascirev.2007.05.007

Tiller, C.C., 1995. Postglacial sediment stratigraphy of large lakes in Greater Yellowstone: scenarios of tectonic and climatic forcing. Master of Science thesis, University of Minnesota, pp. 193.

Tinker, D.B., Romme, W.H., Despain, D.G., 2003. Historic range of variability in landscape structure in subalpine forests of the Greater Yellowstone Area, USA. Landsc. Ecol. 18, 427–439. https://doi.org/10.1023/A:1026156900092

Turner, M.G., Hargrove, W.W, Gardner, R.H., Romme, W.H., 1994. Effects of fire on landscape heterogeneity in Yellowstone National Park, Wyoming. J. Veg. Sci. 5, 731–742. https://doi.org/10.2307/3235886

Turner, M.G., Romme, W.H., and Gardner, R.H., 1999. Prefire heterogeneity, fire severity, and early postfire plant reestablishment in subalpine forests of Yellowstone National Park, Wyoming: Inter. J. of Wildland Fire 9, 21, doi:10.1071/WF99003

Viau, A.E., Ladd, M., Gajewski, K., 2012. The climate of North America during the past 2000 years reconstructed from pollen data. Glob. Planet. Change 84–85, 75–83. https://doi:10.1016/j.gloplacha.2011.09.010

Waddington, J.C.B., Wright, H.E. Jr., 1974. Late Quaternary vegetational changes on the east side of Yellowstone park, Wyoming. Quat. Res. 4(2), 175–184. https://doi.org/10.1016/0033-5894(74)90006-4

Whitlock, C., 1993. Postglacial vegetation and climate of grand teton and southern yellowstone national parks. Ecol. Monogr. 63(2), 173–198. https://doi.org/10.2307/2937179

Whitlock, C., Bartlein, P.J., 1993. Spatial variations of Holocene climatic change in the Yellowstone region. Quat. Res. 39(2), 231–238. https://doi.org/10.1006/qres.1993.1026

Whitlock, C., Dean, W.E., Fritz, S.C., Stevens, L.R., Stone, J.R., Power, M.J., Rosenbaum, J.R., Pierce, K.L., Bracht-Flyr, B.B., 2012. Holocene seasonal variability inferred from multiple proxy records from Crevice Lake, Yellowstone National Park, USA. Palaeogeogr. Palaeoclimatol. Palaeoecol. 331–332, 90–103. https://doi.org/10.1016/j.palaeo.2012.03.001

Whitlock, C., Larsen, C., 2001. Charcoal as a fire proxy. In: Smol, J.P., Birks, J.B., Last, W.M. (eds.), Tracking Environmental Change Using Lake Sediments Vol. 3. Kluwer Academic

Publishers, Dordrecht, p. 507. ISBN: 978-0-306-47668-6

Whitlock, C., Millspaugh, S.H., 1996. Testing the assumptions of fire-history studies: an examination of modern charcoal accumulation in Yellowstone National Park, USA. Holocene. 6(1), 7–15. https://doi.org/10.1177%2F095968369600600102

Whitlock, C., Shafer, S.L., Marlon, J., 2003. The role of climate and vegetation change in shaping past and future fire regimes in the northwestern US and the implications for ecosystem management. For. Ecol. Manage. 178, 5–21. https://doi.org/10.1016/S0378-1127(03)00051-3

Wolfe, A.P., Baron, J.S., Cornett, R.J., 2001. Anthropogenic nitrogen deposition induces rapid ecological changes in alpine lakes of the Colorado Front Range (USA). J. Paleolim. 25, 1–7. https://doi.org/10.1023/A:1008129509322

Zhou, P., Shi, Z., Li, X., Zhou, W., 2020. Response of westerly jet over the Northern Hemisphere to astronomical insolation during the Holocene. Front. Earth Sci. 8, 282.

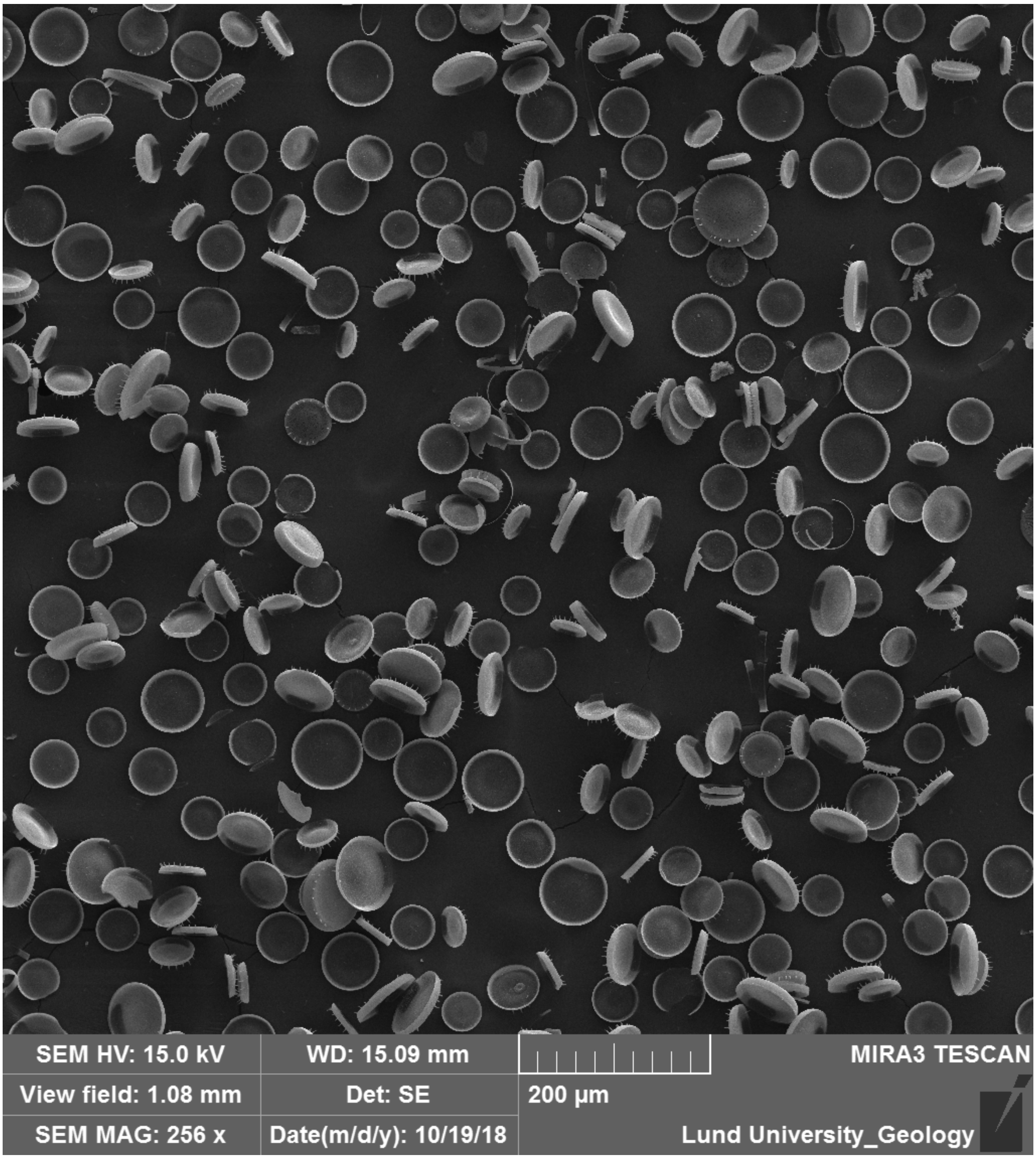

Supplementary material 1: Clean sample (737 cm) for oxygen isotope analysis after treatment. A significant percentage of extracted valves belongs to the species *Stephanodiscus yellowstonensis*. Observations are made with a Scanning Electron Microscope (Tescan Mira3 High Resolution Schottky FE-SEM, Lund University).

Supplementary material 2:

Measurements of oxygen and deuterium isotopes ($\delta^{18}O$ ‰ and δD ‰) in water samples from Lake Yellowstone and its major tributaries during summer 2018. YR: Yellowstone River; YL: surface water samples from Yellowstone Lake. Sample locations are expressed in WGS84.

Identifier	WGS84_longitude	WGS84_latitude	date	δ18O ‰ VSMOW2	δD ‰ VSMOW2
YR outlet	W 110.38120	N 44.56742	28-Aug	-15.9	-126.6
YR outlet	W 110.38686	N 44.59370	25-Aug	-15.8	-126
YR outlet	W 110.38126	N 44.56741	31-Aug	-15.9	-125.7
Pelican Creek	W 110.35702	N 44.55908	28-Aug	-17.9	-137.7
Sedge Creek	W 110.28298	N 44.52377	28-Aug	-17.5	-133.5
Cub Creek	W 110.27699	N 44.48937	26-Aug	-18.1	-134.4
Cub Creek snow	W 110.19575	N 44.50410	28-Aug	-24.8	-190.6
Clear Creek	W 110.27966	N 44.47395	26-Aug	-18.1	-136.1
Meadow Creek	W 110.28607	N 44.42638	26-Aug	-17.6	-134.9
Columbine Creek	W 110.25186	N 44.40100	26-Aug	-18.2	-135.4
Beaverdam Creek	W 110.18056	N 44.32417	24-Aug	-18.5	-138.2
YR inlet	W 110.15687	N 44.29431	24-Aug	-18.6	-137.1
Solution Creek	W 110.50093	N 44.40626	30-Aug	-16.4	-129.4
Big Thumb Creek	W 110.56918	N 44.40517	30-Aug	-17.5	-136.8
Little Thumb Creek	W 110.57966	N 44.43676	28-Aug	-17.8	-136.2
Arnica Creek	W 110.54198	N 44.47728	28-Aug	-19.1	-143.6
Bridge Creek	W 110.43370	N 44.52623	28-Aug	-15.2	-123
YL LW 1	W 110.40639	N 44.52123	23-Aug	-15.4	-125.4
YL LW 2	W 110.37801	N 44.49973	23-Aug	-15.8	-125.5
YL LW 3	W 110.34736	N 44.47348	23-Aug	-15.8	-125.5
YL LW 4	W 110.31525	N 44.44941	23-Aug	-15.8	-125.3
YL LW 5	W 110.30038	N 44.43197	23-Aug	-15.8	-125.0
YL LW 6	W 110.39062	N 44.54403	29-Aug	-15.8	-125.7

Supplementary material 3:

Information on International Measurement Standards VSMOW2 and SLAP2

The two reference materials VSMOW2 and SLAP2 were produced to replace the exhausted reference materials VSMOW and SLAP. Their isotopic compositions for both δ^2H and $\delta^{18}O$ were adjusted to be as close as possible to the predecessor materials. The reference values were assessed from data measured by three laboratories in a calibration exercise measuring the δ^2H and $\delta^{18}O$ data of VSMOW2 and SLAP2 in direct reference to those of VSMOW and SLAP.

IAEA Isotope Hydrology Laboratory, 20 June 2007

Supplementary material 4:

Supplemental Methods

Pollen

A known concentration of *Lycopodium* tracer was added to each sample to calculate pollen concentration (grains cm^{-3}) and influx (grains cm^{-2} yr^{-1}). Residues were preserved and mounted in silicone oil. At least 300 pollen grains were identified at minimum 400× magnification and resolved to the lowest taxonomic level discernible with the reference collection at Montana State University and published atlases (Bassett et al., 1978; Hedberg, 1946; Kapp et al., 2000; Moore et al., 1991). *Pinus* was identified to the subgeneric level when the distal membrane was intact and visible. *Pinus* subgen. *Strobus* was ascribed to *Pinus albicaulis* (i.e., "*Pinus albicaulis-type*"), which grows in the watershed. *P. flexilis* which is more common at low elevations in the GYE, also may have been a contributor. *Pinus* subgen. *Pinus* was ascribed to *Pinus contorta* (i.e., "*Pinus contorta-type*"*)*, given that *Pinus ponderosa* has no native modern occurrences in the GYE (Dorn, 2001; Lesica, 2012). Cupressaceae pollen was prescribed to *Juniperus*-type, and may represent either *J. communis*, *J. scopulorum,* or *J. horizontalis*. Degraded, crumpled, or otherwise unidentifiable pollen grains were classified as "Indeterminate", whereas grains that could not be confidently identified were classified as "Unknown." Vegetation reconstructions for pollen assemblages were aided by a study of modern pollen assemblages from different vegetation types in the Yellowstone region (Iglesias et al., 2018).

Charcoal

Subsamples were disaggregated in 5 wt/vol% $Na_6[(PO_3)_6]$, treated with 5–10 wt/vol% NaOCl, washed gently through a sieve, and then counted under a stereomicroscope (Whitlock and Larsen, 2001). Charcoal accumulation rates (CHAR) were calculated using counts and the median sediment accumulation rate. Then, CHAR was decomposed into a slowly varying background component (BCHAR), which is the long-term trend in biomass burning, and a peak component, which represents fire episodes (one or more fires during the time span). BCHAR was calculated with a 500-year moving average (which kept the local signal-to-noise ratio index above 3 for the entire record). Charcoal peaks were flagged as significant if they registered above the 99th percentile of the local noise distribution of CHAR as defined by a Gaussian mixture model. This percentile was deemed appropriate as it captured known, extremely large fire episodes without introducing erroneous historical fires into the record. Fire-episode frequency was then calculated as an average number of peaks per 100 years, and peak magnitude (particles cm^{-2} yr^{-1}) was used as a proxy of fire-episode size (i.e., total area burned).

Fossil Diatoms

A portion of each individual diatom subsample was added to a vial, weighed to approximately 0.1 g, and immersed in 30% H_2O_2 to remove organic matter (Battarbee, 2003). A known concentration of polystyrene microspheres was added to each subsample to quantify diatom concentration. After processing, each subsample was mounted on a slide with Naphrax optical cement. At least 300 diatom valves were identified to species level and enumerated per slide. Assemblage counts were converted to percentages and plotted. Diatom concentration (number of valves g^{-1}) was calculated using microsphere concentrations, totals, and sample weights.

References

Bassett, I.J., Crompton, C.W., Parmelee, J.A., 1978. An atlas of airborne pollen grains and common fungus spores of Canada. Canada Dep. Agric. Monogr. No. 18, 321 p. http://biblio.uqar.ca/archives/30426283.pdf

Battarbee, R.W., 2003. Diatom Analysis, in: Berglund, B., Ralska-Jasiewicowa, M. (eds.), Handbook of Holocene Palaeoecology and Palaeohyrology. Blackburn Press, Caldwell, NJ, pp. 527–570.

Dorn, R.D., 2001. Vascular Plants of Wyoming, 3rd ed. Mountain West Publishing, Cheyenne, 340 p. ISBN: 281099554709B

Hedberg, O., 1946. Pollen morphology in the genus *Polygonum* L. S. Lat. and its taxonomical significance. Sven. Bot. Tidskr. 40, 371–404.

Iglesias, V., Whitlock, C., Krause, T.R., Baker, R.G., 2018. Past vegetation dynamics in the Yellowstone region highlight the vulnerability of mountain systems to climate change. J. Biogeogr. 45, 1768–1780. https://doi.org/10.1111/jbi.13364

Kapp, R.O., Davis, O.K., King, J.E., Hall, R.C., 2000. Ronald O. Kapp's Pollen and Spores. American Association of Stratigraphic Palynologists Foundation, Dallas, 279 p. ISBN: 0931871050, 9780931871054

Lesica, P., 2012. Manual of Montana Vascular Plants. Botanical Research Institute of Texas Press, Fort Worth, 779P. ISBN: 978-1-889878-39-3

Moore, P.D., Webb, J.A., Collinson, M.E., 1991. Pollen Analysis. Blackwell Scientific Publications, Oxford.

Whitlock, C., Larsen, C., 2001. Charcoal as a fire proxy. In: Smol, J.P., Birks, J.B., Last, W.M. (eds.), Tracking Environmental Change Using Lake Sediments Vol. 3. Kluwer Academic Publishers, Dordrecht, p. 507. ISBN: 978-0-306-47668-6